NASA/TM—2009-215822

An Investigation of Ionic Wind Propulsion

Jack Wilson
ASRC Aerospace Corporation, Cleveland, Ohio

Hugh D. Perkins and William K. Thompson
Glenn Research Center, Cleveland, Ohio

December 2009

NASA STI Program . . . in Profile

Since its founding, NASA has been dedicated to the advancement of aeronautics and space science. The NASA Scientific and Technical Information (STI) program plays a key part in helping NASA maintain this important role.

The NASA STI Program operates under the auspices of the Agency Chief Information Officer. It collects, organizes, provides for archiving, and disseminates NASA's STI. The NASA STI program provides access to the NASA Aeronautics and Space Database and its public interface, the NASA Technical Reports Server, thus providing one of the largest collections of aeronautical and space science STI in the world. Results are published in both non-NASA channels and by NASA in the NASA STI Report Series, which includes the following report types:

- TECHNICAL PUBLICATION. Reports of completed research or a major significant phase of research that present the results of NASA programs and include extensive data or theoretical analysis. Includes compilations of significant scientific and technical data and information deemed to be of continuing reference value. NASA counterpart of peer-reviewed formal professional papers but has less stringent limitations on manuscript length and extent of graphic presentations.

- TECHNICAL MEMORANDUM. Scientific and technical findings that are preliminary or of specialized interest, e.g., quick release reports, working papers, and bibliographies that contain minimal annotation. Does not contain extensive analysis.

- CONTRACTOR REPORT. Scientific and technical findings by NASA-sponsored contractors and grantees.

- CONFERENCE PUBLICATION. Collected papers from scientific and technical conferences, symposia, seminars, or other meetings sponsored or cosponsored by NASA.

- SPECIAL PUBLICATION. Scientific, technical, or historical information from NASA programs, projects, and missions, often concerned with subjects having substantial public interest.

- TECHNICAL TRANSLATION. English-language translations of foreign scientific and technical material pertinent to NASA's mission.

Specialized services also include creating custom thesauri, building customized databases, organizing and publishing research results.

For more information about the NASA STI program, see the following:

- Access the NASA STI program home page at *http://www.sti.nasa.gov*

- E-mail your question via the Internet to *help@sti.nasa.gov*

- Fax your question to the NASA STI Help Desk at 443–757–5803

- Telephone the NASA STI Help Desk at 443–757–5802

- Write to:
  NASA Center for AeroSpace Information (CASI)
  7115 Standard Drive
  Hanover, MD 21076–1320

NASA/TM—2009-215822

An Investigation of Ionic Wind Propulsion

Jack Wilson
ASRC Aerospace Corporation, Cleveland, Ohio

Hugh D. Perkins and William K. Thompson
Glenn Research Center, Cleveland, Ohio

National Aeronautics and
Space Administration

Glenn Research Center
Cleveland, Ohio 44135

December 2009

This work was sponsored by the Fundamental Aeronautics Program at the NASA Glenn Research Center.

Level of Review: This material has been technically reviewed by technical management.

Available from

NASA Center for Aerospace Information
7115 Standard Drive
Hanover, MD 21076–1320

National Technical Information Service
5285 Port Royal Road
Springfield, VA 22161

Available electronically at http://gltrs.grc.nasa.gov

An Investigation of Ionic Wind Propulsion

Jack Wilson
ASRC Aerospace Corporation
Cleveland, Ohio 44135

Hugh D. Perkins and William K. Thompson
National Aeronautics and Space Administration
Glenn Research Center
Cleveland, Ohio 44135

Abstract

A corona discharge device generates an ionic wind and thrust, when a high voltage corona discharge is struck between sharply pointed electrodes and larger radius ground electrodes. The objective of this study was to examine whether this thrust could be scaled to values of interest for aircraft propulsion. An initial experiment showed that the thrust observed did equal the thrust of the ionic wind. Different types of high voltage electrodes were tried, including wires, knife-edges, and arrays of pins. A pin array was found to be optimum. Parametric experiments, and theory, showed that the thrust per unit power could be raised from early values of 5 N/kW to values approaching 50 N/kW, but only by lowering the thrust produced, and raising the voltage applied.

In addition to using DC voltage, pulsed excitation, with and without a DC bias, was examined. The results were inconclusive as to whether this was advantageous. It was concluded that the use of a corona discharge for aircraft propulsion did not seem very practical.

1.0 Introduction

The ionic wind is the creation of movement of air, or other fluids, by means of a corona discharge. It was studied scientifically as long ago as 1899 by Chattock (Ref. 1), although its existence was known even before that. More recently, it has been used as a mechanism to pump liquids (Ref. 2), and was investigated as a propulsion technique in air by Christenson and Moller (Ref. 3). It is also the basis of a commercially available device for air purification, called the Ionic Breeze. Thus it seemed worthwhile to revisit the question raised by Christenson and Moller, namely, whether the corona discharge can be used for aircraft propulsion.

A corona discharge is a discharge in air between a highly curved electrode and a less curved, or even plane electrode. It is characterized by high voltage, but low current. If the voltage is raised too high, it converts into a spark. Thus there is a limited range of power over which it operates. Consequently it does not seem likely that ionic wind engines could be used to propel large aircraft, but there may be some applications for which it is suited. Possible examples are aircraft using solar power to generate electricity, which could be transformed to high voltage to power the corona discharge. One such is the unmanned Helios airplane (Ref. 4), which has the entire upper surface of its wing covered with solar cells. The cells produce a maximum of 40 kW of electricity, which in the prototype version power twelve electric motors turning propellers, using 21 kW of power. A rough estimate of the thrust of Helios is about 500 N, for a thrust to power ratio, θ, of 25 N/kW. Thus if the maximum thrust to area ratio, ϕ, seen by Christenson and Moller, namely 4.5 N/m^2, were used, the engine would have a frontal area of 111 m^2. The span of Helios is 75 m, so a full span engine would have to be 1.5 m high. Whilst this is large, it does not seem impossible, and increases in efficiency could make the engine size more acceptable. Moreover, two or more stages (i.e., sets of electrode pairs) could be stacked to reduce the frontal area by as many stages as used. Note though that the values for θ and ϕ quoted for Christenson and Moller do not occur at the same voltage; maximum θ is not consistent with maximum ϕ.

Another example might be for proposed stationary blimps for communication purposes, as e.g., the Lockheed Martin High Altitude Airship (Ref. 5), or HAA. This airship is planned to be 150 m long, with a diameter of 46 m. If solar cells were placed on the upper surface, covering one quarter of the circumference, over half the length of the airship, then at the same solar efficiency as the cells on Helios, they would produce about 500 kW. Assuming a corona discharge thrust to power ratio of 20 N/kW, this would generate 10,000 N of thrust. The announced solar power for the HAA will be amorphous silicon photovoltaic cells, which have a rather low efficiency, and only 10 kW of electrical power is projected. This seems low, since the much smaller Goodyear blimps (59 m long by 15 m diameter) use two 158 kW internal combustion engines for propulsion. Similar motors for a proposed Large Crane Airship (Ref. 6), would generate about 2700 N each, at a thrust to power ratio of 18 N/kW.

In summary, even though the efficiency of corona discharge engines is low, they have demonstrated the same thrust to power ratios as more conventional engines. The frontal area is large, but can be reduced by staging, and possibly by improvements in technology.

If values of $\theta = 20$ N/kW, and $\phi = 20$ N/m^2, could be attained simultaneously, corona discharges might be useful for the applications above, and will be taken as goals.

However, corona discharge engines probably will not be useful at high altitude, as experiments at Blaze Laboratories (Ref. 7) have shown the corona discharge thrust decreases as density decreases, i.e., as altitude increases. Another unknown is the effect of the vehicle forward velocity. The air velocity generated by a corona discharge is very low, of the order of 2 m/sec. There is a report of operating a corona discharge in high velocity (up to Mach 1.3) flows (Ref. 8), when changes in the discharge characteristics were noted, but thrust was not measured. It is encouraging that a corona discharge can function in a high speed flow, but whether the thrust still exists at these velocities remains to be seen.

The effort described in this report was undertaken with several objectives that need to be addressed if ionic wind devices are to be used for aeronautical propulsion. These were; (a) to determine whether the thrust generated by a corona discharge is caused by the ionic wind generated, (b) to investigate geometrical and voltage changes to see under what conditions the goals of $\theta = 20$ N/kW, and $\phi = 20$ N/m^2 could be achieved, and (c) to use pulsed voltages to see whether they are beneficial to corona ionic wind generation.

2.0 Corona Discharge Properties

A corona discharge takes place between an electrode with a sharply curved surface, e.g., a point or a fine wire, and a larger, less curved surface, or even a plane. The point or wire is called the emitter electrode, and can be charged either negatively or positively. The other electrode is called the collector electrode, and is grounded. The corona is a form of glow discharge in which, except for a small region around the emitter, the current is carried entirely by ions. Voltages are in the 10 to 50 kV range in atmospheric pressure air. The small size of the emitter creates a very large local electric field in the vicinity of the tip or the wire, of the order of 10^7 V/m. Such high fields give rise to field emission of electrons. If the emitter is positively charged, the electrons will return to the emitter, but in the process, they will undergo collisions with air molecules, creating positively charged ions. These ions will be repelled by the emitter, and be attracted to the collector. In their passage to the collector, ions will impact air molecules, giving them momentum, and thereby generating the ionic wind. The region in which the ions are created is very small compared with the distance between the emitter and the collector, so that most of the discharge region is dominated by ion current. The thickness, δ (mm), of the ionization region can be calculated from (Ref. 9)

$$\delta = \sqrt{a} \tag{1}$$

where a (mm) is the radius of the wire, or tip radius of a point.

If the applied voltage is raised too much, and approaches the spark-breakdown voltage for that gap, the glow discharge will change into a spark.

Christenson and Moller (Ref. 3) showed that the thrust generated by the ionic wind in air, T (Newtons), can be written as

$$T = I\ d/\mu \tag{2}$$

where I = current in the discharge (amps), d is the gap between emitter and collector electrodes (metres), and μ the ion mobility (m^2/V-sec).

Given the thrust, the thrust per unit power, θ, is

$$\begin{aligned} \theta &= T/IV \\ &= (d/V)/\mu \\ &= 1/E\mu \end{aligned} \tag{3}$$

in which V is the applied voltage, and E the average electric field, defined as $E = V/d$. This last equation shows the difficulty with using the ionic wind as a propulsion scheme, since in order to obtain a high thrust to power ratio, the electric field must be low, which implies low current, and hence low thrust by Equation (2). An alternative is to have low mobility. The mobility of air is known, and depends on humidity (Ref. 10), but only varies from a value of 2.15×10^{-4} m^2/V-sec for dry air to 1.6×10^{-4} for saturated air. Christenson and Moller were aware of this, but proposed that the effective mobility might be decreased by pulsing the applied voltage. There does not appear to be any record of their having accomplished this. From their experiments, Christenson and Moller concluded that the propulsion efficiency was about 1 percent, which is too low to be practical. Their maximum measured thrust was about 0.45 N, with a flow area of roughly 0.1 m^2, and their optimum thrust to power ratio was 21 N/kW. The only geometrical variable in the experiment was the distance between the electrodes.

Equation (2) can be derived very simply by assuming, as did Christenson and Moller, that the electric field is uniform in the main part of the corona discharge, with an applied voltage of V (volts). Since no more ions are created once the ions have left the high field region around the tip, the product of ion density, n_i and discharge cross-section, A, will be constant. Every ion will experience an electrostatic force, T_i, given by

$$T_i = e\,E \tag{4}$$

where e is the unit charge, and of course there is an equal and opposite force on the electrodes. The total force of all the ions on the electrodes is then

$$T = N\,T_i = N\,e\,E \tag{5}$$

in which N, the total number of ions in the discharge, is simply $N = n_i\,A\,d$. The discharge current is given by

$$I = n_i\,e\,v_i\,A \tag{6}$$

where v_i is the average ion velocity, which is given by $v_i = \mu E$. It follows that the total force on the electrodes is:

$$\begin{aligned} T &= N\,e\,E \\ &= n_i\,A\,d\,e\,E \\ &= (n_i\,e\,v_i\,A)\,d\,E/\mu E \\ &= I\,d/\mu \end{aligned} \tag{7}$$

in agreement with Equation (2). This shows that the thrust force associated with the ionic wind is simply electrostatic repulsion of the anode by, and attraction of the cathode to, the cloud of ions in the discharge.

The velocity of the ions in the derivation above was dependent on the ion mobility, which is determined by collisions of the ions with the air through which they are travelling. The ionic wind itself is created at each collision of an ion with an air molecule, which impedes the motion of the ion towards the cathode, and accelerates the air towards the cathode. A simple model of the collisions will illustrate this. The ions are in a uniform field, and so will accelerate at a constant acceleration, a, given by;

$$a = eE/m_i \tag{8}$$

where m_i is the mass of the ion. After a distance λ, i.e., the mean free path of the ions in air, the ion will collide with an air molecule. If it is further assumed that in this collision the ion is brought to rest, and the air molecule is given all the momentum that the ion had prior to the collision, then the ion will have traveled the distance λ in a time t such that:

$$\lambda = a t^2/2 \tag{9}$$

and the average velocity of the ion is

$$\begin{aligned} v_i &= \lambda/t \\ &= a t/2 \\ &= (e E/2 m_i)\sqrt{2 m_i \lambda/eE} \\ &= E\sqrt{e\lambda/2 m_i E} \end{aligned} \tag{10}$$

but v_i/E is the mobility μ, so that

$$\mu = \sqrt{e\lambda/2 m_i E} \tag{11}$$

The result that μ is proportional to the inverse square root of the field agrees with results for ions in air at high electric field quoted by Sigmond (Ref. 11). In travelling the distance d between emitter and collector, each ion will undergo d/λ collisions. At each collision the ion has momentum $2m_i v_i$, which it gives to the air molecule. This assumes head-on collisions of equal mass ions and air molecules. Thus the total momentum given to the air per second, i.e., the force accelerating the air, F, is:

$$F = n\, 2 m_i v_i\, d/\lambda \tag{12}$$

in which n is the number of ions arriving at the collector per second, $= I/e$. Inserting this, and Equation (10) for v_i, into Equation (12), the force accelerating the air is:

$$F = I\, d\sqrt{2 m_i E/e\lambda} \tag{13}$$

and using Equation (11)

$$F = I\, d/\mu \tag{14}$$

Thus it is seen that the force accelerating the air, i.e., the momentum given to the ionic wind, is the same as the thrust on the electrodes, which is itself the reaction to the electrostatic force on the ions.

Christenson and Moller (Ref. 3) used multiple sharp points, but were not explicit in stating how many, though a sketch of their apparatus seemed to indicate that they might be spaced several centimeters apart. The study by Chattock (Ref. 1) showed that the diameter of the discharges he studied, which were between a single sharp point and a flat plane, was less than about 1 cm. Thus it seems as though the

needles could possibly be spaced about this distance apart, which would significantly reduce the frontal area needed for a given thrust. One objective of the present investigation was to vary the electrode geometry to see under what conditions better thrust to frontal area can be achieved, and at what thrust to power ratio, in order to evaluate whether there could be any practical use of such devices. A second objective was to examine pulsing the applied voltage to see whether this results in increased thrust to power ratio. In addition to these objectives, some tests were made to determine whether or not the thrust produced by a corona discharge is indeed connected to the ionic wind generated by the discharge.

3.0 Experiments on Electric Thrust and Ionic Wind

3.1 Ionic Wind Tests

There have been questions as to whether the thrust generated by a corona discharge is due to the ionic wind created, or due to some other mechanism, possibly an interaction between gravitation and electromagnetism (Refs. 12 to 14). These have been partially answered by Tajmar (Ref. 15). In an elegant experiment, Tajmar enclosed a corona discharge entirely inside a box suspended on wires. No motion of the box was observed when the discharge was turned on, even though a very sensitive motion detection system was used. Since the enclosure blocked the ionic wind, but should have no effect on other mechanisms, this indicates that the ionic wind generates the thrust. It does not however, show quantitatively that the thrust is identical to the momentum of the ionic wind. Consequently, two tests were performed which do lead to this conclusion.

3.2 Description of the Apparatus

Two different corona discharge "lifters" were used in the experiments. The first was a hexagonal lifter of the type described by Naudin (Ref. 16), consisting of a hexagon made up from six equilateral triangles with sides 150 mm in length. Each side had a collector electrode on the bottom, made of horizontal bars of basswood, separated vertically by about 15 mm, and enclosed in aluminum foil. Spaced 32 mm above the collector electrodes were 0.07 mm diameter wires constituting the emitter electrodes; Figure 3.1. With a total weight of 9 g, it lifted off the ground when a voltage of 24.6 kV was applied to the emitter electrodes, generating a current of 1.4 mA. In the tests, it was mounted on an Ohaus, Scout-Pro digital balance, with a range of 400 g, and a resolution of 0.1 g. First it was mounted on an open support which rode directly on the balance, and then subsequently a shield was interspersed between the lifter and the balance, which blocked the ionic wind from impacting the balance. The support legs passed through small holes in the shield. The balance was zeroed with the lifter removed, and so read the weight of the lifter, when the latter was replaced on the support, without any current flowing.

The second lifter, called a box lifter, had a set of 13 parallel ground electrodes, each 150 mm in length, and having a 4.5 mm radius leading edge, with an 8 mm web behind it, which was wrapped in aluminum foil to make the electrode conductive. They were installed in a square styrofoam duct, 150 mm on each side, and 50 mm high, open at the top and bottom, with the leading edges all in the same plane, normal to the height, which was situated 15 mm from the bottom of the duct; Figure 3.2. The high voltage, or emitter, electrode consisted of copper wires, 0.075 mm in diameter, stretched across the duct, one above each ground electrode, in a plane 32 mm above the ground plane.

Both lifters were powered by a Glassman model EQ30P40 DC High Voltage Power Supply, with a maximum voltage and current capability of 30 kV and 40 mA, respectively. The voltage and current were measured with the meters built-in to the supply. The ammeter only reads every 0.1 mA, however, by setting the voltage so that the current just changed from one reading to the next, an accuracy of maybe 0.02 mA is possible, corresponding to a possible error of 0.1 g in the force. With the resolution of the balance at 0.1 g, the accuracy of the measurements is about 0.2 g, which is sufficient for the purposes of this study.

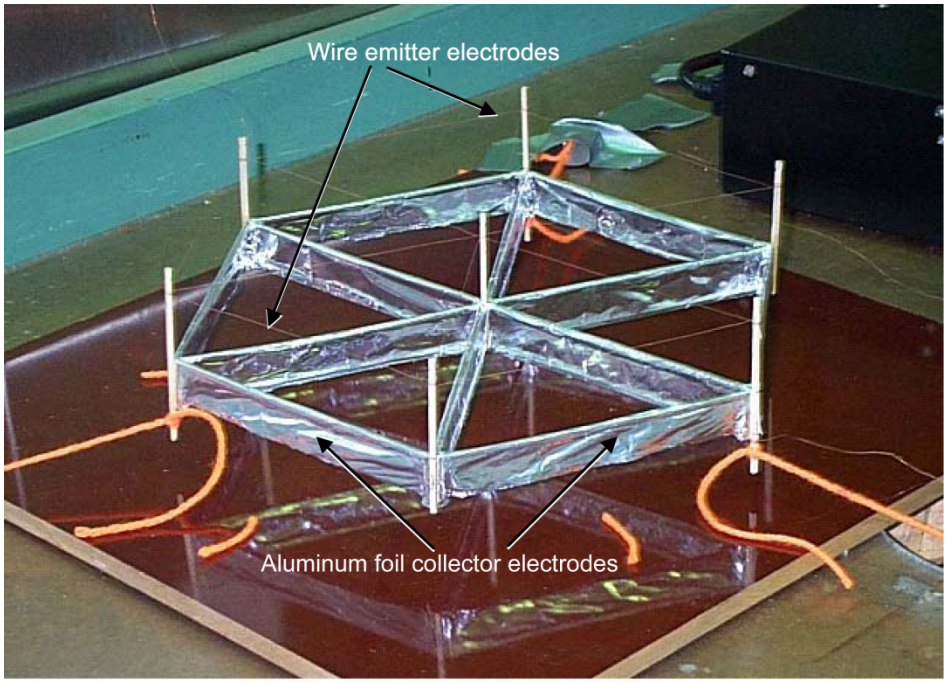

Figure 3.1.—Photograph of the “hexalifter”. As can be seen from the reflections in the phenolic board of the bottom of the tethered vertical posts, the lifter is in “flight”.

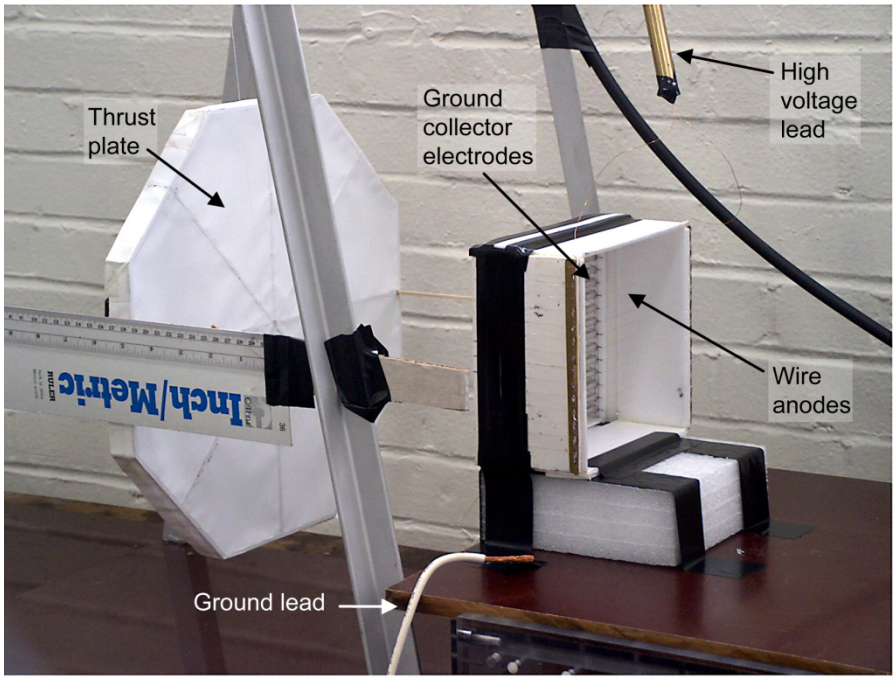

Figure 3.2.—Photograph of the thrust plate and the box lifter.

For the second experiment, the ionic wind was measured using a ballistic thrust plate, consisting of a hexagonal plate 330 mm width, made out of thin basswood strips, covered with ordinary paper; Figure 3.2. Two horizontal shafts passed through the plate, and threads were attached to the ends of the shafts to give a four wire support, so that the plate remained normal to the horizon when moving. At their other end, the threads were attached to a support structure, to which a scale was also fastened, against which the movement of the plate could be read. The weight of the thrust plate and shafts, M, was 23.4 g, and the length of the threads, ℓ, was 47.6 cm. Movement of the plate, δ, was read off a scale attached to the support structure. The thrust plate, scale, and box lifter, mounted on its side, are shown in Figure 3.2.

3.3 Description of the Experiments

In the first experiment, the hexagonal lifter was placed on the support, riding on the balance, which then indicated the weight of the lifter. There was no blocking shield between the lifter and the balance. The power supply was turned on, and the voltage was increased in steps, each step corresponding to an increase in current of one tenth of a milliamp. The balance reading was noted, and is shown in Figure 3.3, as a function of current, as the upper trace. At a current of 1.4 mA, the lifter rose from the balance. Following this test, the blocking shield was placed between the lifter and the balance, and the test repeated. The balance reading was now the lower trace in Figure 3.3.

In the second experiment, the box lifter was placed on the balance, with the shield in place, and again a force versus current trace was obtained. Following this, the lifter was mounted so that its axis was horizontal, and placed so that its exhaust was directed at the thrust plate, with the axes of the lifter and thrust plate coinciding, as in Figure 3.2. The current was brought up in stages as before, but now the deflection of the thrust plate was measured as a function of current. The plate deflection is, of course, related to the thrust of the ionic wind. In Figure 3.4, the thrust measured by the balance is compared with the force of the ionic wind on the thrust plate.

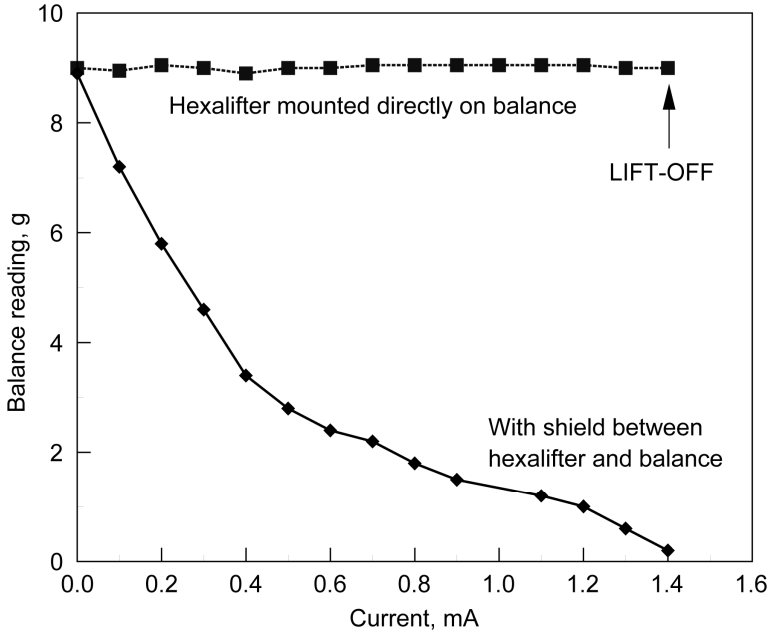

Figure 3.3.—Balance readings versus current for the hexalifter mounted directly on the balance, and with a shield between the hexalifter and the balance.

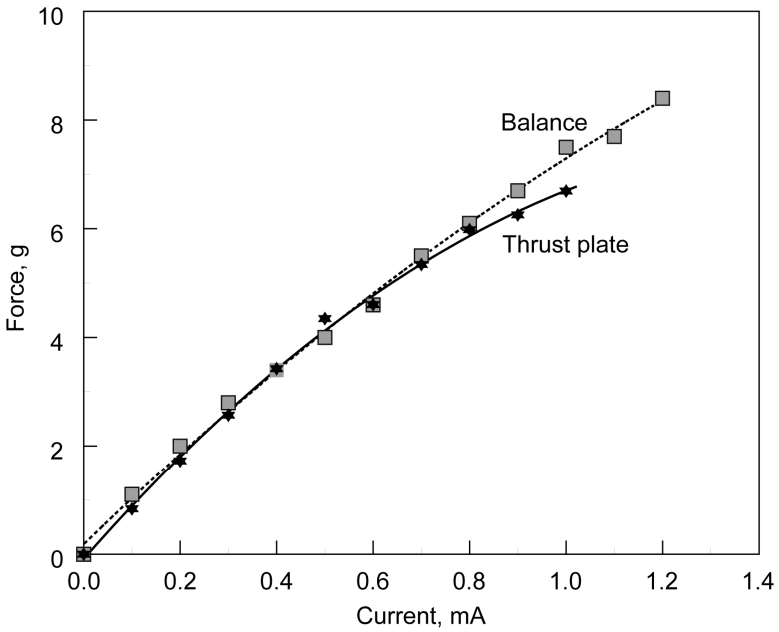

Figure 3.4.—Measurements of the force exerted by the box lifter on the balance and on the thrust plate as a function of current.

3.4 Interpretation of the Experimental Results

In the first experiment, the load on the balance, L, without a shield in place will be

$$L = (W - T_e) + T_{iw} \tag{15}$$

in which the term in brackets is the weight of the lifter, W, minus the electric thrust, T_e, and the second term, T_{iw}, is the force on the balance due to the momentum of the ionic wind. If the electric wind momentum equals the electric thrust, they cancel, and the balance reading remains at the weight of the lifter as the thrust increases, as observed. However, when the ionic wind is blocked, the force on the balance is simply the term in brackets, which should go to zero when the lifter rises. This is what is seen, as shown in the lower curve in Figure 3.3.

In the first phase of the second experiment, the balance again read (W–T_e), from which T_e is obtained as a function of current, knowing W for the lifter. It is T_e that is plotted against current in Figure 3.4. The displacement of the thrust plate, δ is converted into the force on the thrust plate, F, by the formula:

$$F = M \tan(\text{arcsine}(\delta/\ell)) \tag{16}$$

This force F must be equal to the thrust of the ionic wind, T_{iw}. As can be seen from Figure 3.4, except at the upper values of current, the values of T_e from the balance, and T_{iw} from the thrust plate are in very good agreement. The discrepancy at the larger values of current is probably due to the fact that at large deflections, as the thrust plate moved, it also moved upwards, and, despite the four-point support, also tilted.

That, to the accuracy of this experiment, the balance reading did not change as current increased when the hexalifter was mounted directly on the balance, shows that the electric lift equals the thrust from the ionic wind, i.e., that $T_e = T_{iw}$. That it did change when the shield was placed between the lifter and the balance, going to zero at the current at which the lifter rose from the support, shows that at this point, the electric thrust T_e equals the hexalifter weight, and hence, since, from above, the electric thrust equals the

ionic wind thrust, the latter equals the weight of the lifter also. In other words, the ionic wind thrust is identical to the lift created by a corona discharge.

Similarly, for the box lifter, since the curve of electric thrust versus current is in good agreement with the curve of ionic wind thrust from the thrust plate, again the electric lift force is equal to the ionic wind force. The thrust plate is made of nonconductive, nonmagnetic materials, and so is responsive only to wind forces, so that what it measures is thrust due to the ionic wind. Since the thrust at a given current is the same whether the lifter is horizontal or vertical, any interconnection between electromagnetism and gravitation seems implausible.

4.0 Comparison of Pin and Wire Emitters

4.1 Pin Optimization

From the results with the hexagonal lifter, it is seen that the thrust/power is equal to 2.6 N/kW when the device lifts from the support. This is considerably less than the best values seen by Christenson and Moller (Ref. 3). One major difference is that Christenson and Moller used pins rather than wires. This suggests that pins are superior to wires. In using pins, there is an array of variables that can affect the lifter performance, namely, the gap d, the number of pins per electrode, the separation between electrodes, s, the number of electrodes, and the radius of the pin tip, r. Experiments were made to try to determine optimum values for these quantities.

To achieve this, the box lifter was equipped with emitter electrodes made of thin brass sheets, to which regular household pins were soldered, as shown in Figure 4.1(a). The lifter was mounted on supports on the balance, as described in Section 3, with the shield in-between. The balance reading together with current and voltage readings were taken as the voltage was gradually increased. From the readings, and the measured value of the pin point to the collector leading edge distance, d, the values of θ and E could be calculated.

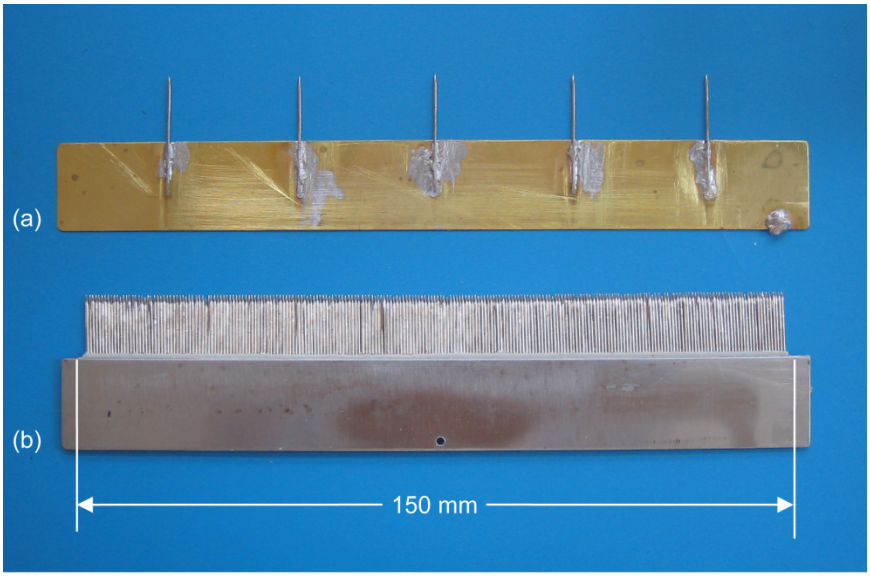

Figure 4.1.—Photographs of (a) an emitter electrode with five pins, and (b) the brush electrode with two hundred fifty-four pins.

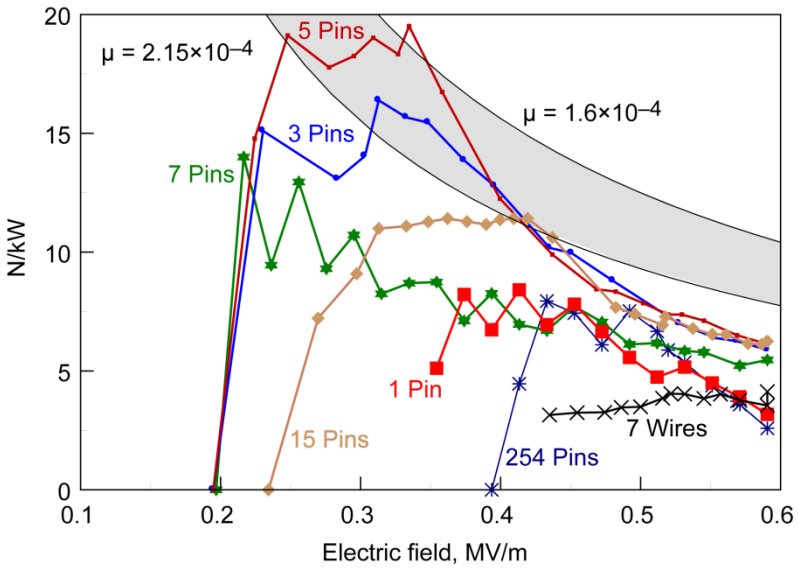

Figure 4.2.—Performance of a single emitter electrode with differing numbers of pins. The pins are household pins, with a gap d = 50 mm. Also shown is the performance of an array of seven wires.

4.2 Optimum Number of Pins

In assessing the optimum number of pins per electrode, a single emitter electrode was used, with positive voltage on the emitter. The gap was fixed at a value of d = 50 mm, and household pins were used. Various numbers of pins were used, including an electrode for which as many pins as possible (254) were placed side by side; Figure 4.1(b). Similar electrodes have been used in other discharge schemes (Ref. 17). The objective was to generate a large current, and hence, according to Equation (1), a large thrust. The results for all the various numbers of pins, presented as θ versus E are given in Figure 4.2. For comparison, results from an array of wire emitters are also shown. Additionally given is the area bounded by Equation (2), using the mobility for dry and saturated air, shown as the shaded region.

The results show that there is indeed an optimum number of pins, or more likely, an optimum spacing between pins. The number of pins is five, corresponding to a spacing of 29 mm. As the number of pins increases, it is noticeable that there appears to be a critical electrical field, and hence a critical voltage, for onset of thrust, which increases as the pins get closer together. It is probable that close spacing affects the field distribution around the pins, lowering the local field at each pin tip. The array of wires shows poor performance compared with pins.

4.3 Optimum Electrode Separation

In an early test using fifteen pins per electrode, experiments were run with three emitter electrodes at four electrode separations of s = 9.5, 19, 38, and 57 mm, at a current of 0.1 Ma. The results are given in Table 1.

TABLE 1.—RESULTS OF TESTS IN WHICH THE SEPARATION OF THREE EMITTERS WAS VARIED

Separation, mm	Voltage, kV	Thrust, N	θ, N/kW
9.5	25.3	0.02	0.79
19	24.3	0.02	0.82
38	22.4	0.023	1.03
57	22.1	0.02	0.90

Although the voltage to achieve 0.1 mA is decreasing monotonically as the electrodes are separated, indicating again that there is an interaction between the electrodes when they are close, the thrust is higher at a separation of 38 mm than it is at 57 mm, resulting in a higher value of θ. This was observed also at a current of 0.2 mA. It is concluded that 38 mm is an optimum electrode separation. With this separation, the maximum number of emitter electrodes that could be fitted into the duct, and leave an equivalent space between the outer electrodes and the wall was three.

4.4 Pin Tip Radius and Critical Voltage

It was pointed out above that there is a critical voltage for the onset of thrust. It is well-known that there is a critical voltage for onset of current in a corona discharge (Ref. 18), dependent on the pin tip radius. It can be determined by plotting I/V against V, as will be shown below in Section 5. Such measurements were made for an array of seven emitter electrodes, with seven pins each, and an array of three emitters with five pins each, both using household pins, as well as an array of three emitters with tungsten pins. The tungsten pins were machined to give a much smaller tip radius than the household pins. A single electrode with two hundred fifty-four household pins was also tested. The results are in Table 2.

TABLE 2.—CRITICAL VOLTAGES FOR DIFFERENT ELECTRODE ARRANGEMENTS

Electrode array	Tip radius, r, μm	Critical voltage, kV
One electrode with two hundred fifty-four pins	10	12.5
Seven electrodes with seven household pins	10	10
Three electrodes with five household pins	10	7.5
Three electrodes with five tungsten pins	2	5

According to Cobine (Ref. 9), the critical voltage depends only on the tip radius, and not on the gap size. However, he was only considering a single point electrode. It appears that not only the tip radius, but also the geometry, of an array of pins can affect the critical voltage.

The array of three emitter electrodes with five pins has a lower critical voltage than does the array with seven electrodes with seven pins each. This is undoubtedly why the former array exhibits better performance. The electrode with two hundred fifty-four pins has the highest critical voltage, and the poorest performance. From the point of view of the critical voltage, it is obviously desirable to have as small a tip as possible. In practice, too small a radius may be ineffective, since there will be erosion of the point in the discharge. Figure 4.3 is a photograph of three pins. The pin on the left is a household pin, before use, in the middle is a tungsten pin with a new point, and on the right is a tungsten pin that had been used in several experiments. There is clearly erosion of the sharp pin. Whether the rate of erosion eventually stabilizes at some radius, and whether the rate of erosion is reduced at low currents is not known, but seems possible. This is an area that needs more study. Christenson and Moller (Ref. 3) also reported tip erosion, but they were using aluminum points, which may erode more rapidly than tungsten. It is possible that there may be better materials than tungsten for the needles.

4.5 Optimum Gap Size

Using three emitter electrodes with five tungsten pins and an electrode separation of 38 mm, a test series was run in which voltage-current characteristic data were taken. Thrust was measured as well as the current and voltage. Various values of the gap were used, namely 19, 44, 57, 70, and 95 mm. Values of θ and E calculated from this data are plotted in Figure 4.4. The shaded area is the range of theoretical values of θ calculated from Equation (2), bounded by curves for the dry and saturated air mobilities. The experimental values do seem to be bounded by the dry mobility curve. It also appears that there is an optimum gap of somewhere between 57 and 70 mm. The largest and smallest gaps are clearly worse.

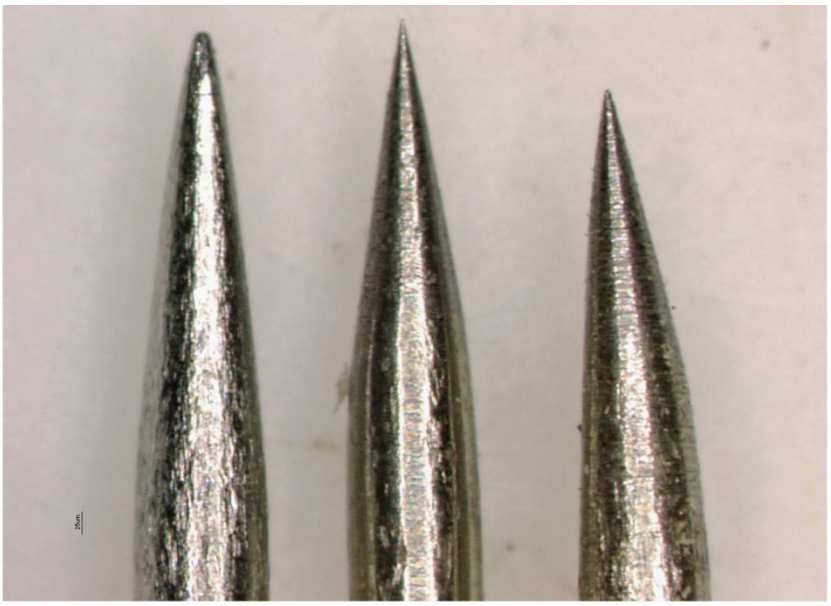

Figure 4.3.—Photograph of three pins. On the left is a household pin, in the middle is a new tungsten pin, and on the right is a tungsten pin that has been used.

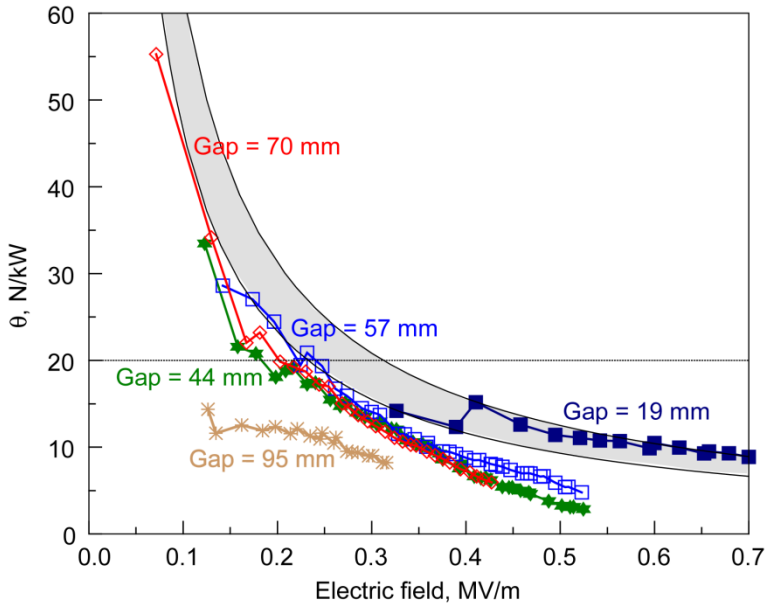

Figure 4.4.—Plot of θ versus electric field for different gaps. The emitter electrode array is three electrodes with five tungsten pins each. The shaded area is the region bounded by the curves of $\theta = 1/\mu E$ with the values of mobility for dry and saturated air.

However, it is not possible to be definite about the optimum gap, since the values at the left hand side of the curve are somewhat suspect. This is because the smallest reading on the balance used is 0.1 g. Experimentally, the thrust is called 0.1 g when the balance reading increases by 0.1 g over the reading with no current. However, if the lifter weighed, say, 50.09 g with no current, the balance would read 50.0 g; a thrust of 0.01 g would change the balance reading to 50.1 g, and so would be considered to be a thrust of 0.1 g. As the thrust increases, this zero error becomes less of a problem, so points to the right of Figure 4.4 are accurate.

Equation (3) does not appear to have any dependence on the gap, since θ only depends on the inverse of the electric field multiplied by the mobility, and will be increased by reducing the electric field. The electric field is V/d, and if d is made small, the field gets large. Compensating for this by reducing the voltage is limited because V cannot be reduced below the critical voltage V_c. Thus any given electrode array, and gap, can only operate at fields greater than V_c/d. In order to generate θ = 20 N/kW in dry air, according to Equation (3), the field required is 0.233 MV/m, so with a critical voltage of 5 kV (the lowest achieved so far in this report), d = 21.5 mm. This is only slightly larger than the 19 mm actually tested. But, in fact, if the voltage is exactly equal to the critical voltage, the current, and hence the force goes to zero: a larger voltage is required to generate thrust, which then will be at a lower value of θ.

4.6 Dependence of Thrust on Gap Size

Equation (2) shows that the thrust is proportional to the gap size. In the derivation of this equation it is assumed that the electric field is uniform between the electrodes. This is not true in reality. If Equation (2) were true, then a plot of T/d against I would be the same straight line for all values of d. The data of Section 4.4 were used to make such a plot, and it was found that the slope of the lines was different for each value of d. Instead it was assumed that an equation of the form,

$$T = B\,d^{n}\,I/\mu \tag{17}$$

where B is a constant, would be appropriate. For each of the five different values of d used in the tests, a value of $T/(I/\mu)$ was determined from the data. By assuming a value for n, B can be found for each value of d. This was repeated at different values of n until the minimum value of $\sqrt{\Sigma\left(B-\overline{B}\right)^2}$ was obtained. The minimum was found at n = 0.56, B = 0.238. In Figure 4.5, $T/0.238\ d^{0.56}$ is plotted against I/μ for all the values of d used in the experiment. If this is the correct formulation, all the curves should fall on top of one another. Whilst there is some scatter, the curves do overlap reasonably well, at low current, which, fortunately, is the region which will give high values of θ.

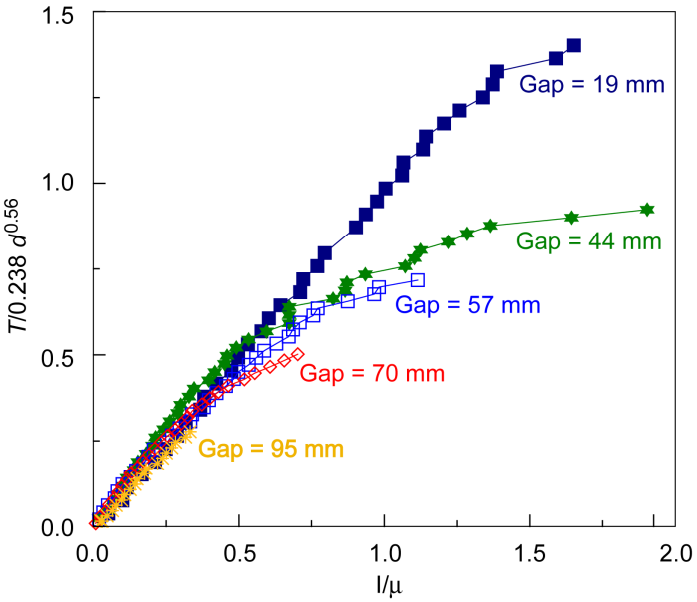

Figure 4.5.—Thrust divided by $Bd^{0.56}$ plotted against current divided by ion mobility. For small currents, the slope is unity, showing that these quantities are equal.

5.0 Discharge Characteristics

5.1 Current-Voltage Relation

It would be useful to have an analytical expression for the current-voltage relationship. Raizer (Ref. 18) has derived such an expression for the case of a corona discharge between concentric cylinders, of radii r and R, respectively, with an applied voltage, V, namely:

$$I = 2\mu V\left(V - V_c\right)/R^2 \ln\left(R/r\right) \tag{18}$$

V_c is the critical voltage, below which no current will flow. The case of points discharging to a plane surface is more appropriate for most of the work reported here. Although Raizer gave the equation for the electrostatic field for the case of a point discharging to a plane, he did not use it to derive an equation equivalent to Equation (18) for that case. The electric field for the point/plane case is:

$$E\left(x\right) = 2V/\left(r + 2x\right)\ln\left(2d/r + 1\right) \tag{19}$$

where x is distance from the point towards the plane, r is the radius of the point, and d is the distance from the point to the plane. The current is given by:

$$I = n_i\, e\, \mu\, E\left(x\right)A\left(x\right) \tag{20}$$

where n_i is the ion density, e the electronic charge, and $A(x)$ is the area of the discharge. By substituting into Poisson's equation, $dE(x)/dx = 4\pi\, n_i\, e$, assuming the discharge area has a relationship with x given by $A(x) = A\, x^m$, and integrating, the field becomes:

$$E\left(x\right) = 4\,\pi\, I\,\left[\ln\left(2d/r\right)/\mu V\right]x^{\left(2-m\right)}/\left(2-m\right)A \tag{21}$$

and by integrating the field from $x = 0$ to d, which gives the voltage,

$$V = 4\,\pi\, I\,\left[\ln\left(2d/r\right)/mV\right]d^{\left(3-m\right)}/\left(3-m\right)\left(2-m\right)A + V_c \tag{22a}$$

The term V_c appears because $V = V_c$ when the current is zero. Inverting this expression, the desired equation for the current becomes:

$$I = \mu V\left(V - V_c\right)\left(3-m\right)\left(2-m\right)A/\left(4\pi d^{\left(3-m\right)}\ln\left(2d/r\right)\right) \tag{22b}$$

$$= K\,\mu V\left(V - V_c\right)/\left[d^{\left(3-m\right)}\ln\left(2d/r\right)\right] \tag{22c}$$

In Equation (22c) all the constants, except for μ, have been lumped into the single constant K. Not surprisingly, this equation is similar to Equation (18). One aspect of this equation is that by plotting I/V against V, the intercept on the abscissa gives V_c. This has been done using data taken with the box lifter. For this experiment, the wire emitters were replaced with three emitter electrodes each consisting of a brass strip onto which five sharpened pins were soldered, as shown in Figure 4.1(a), together with four brass collector electrodes. The collector electrodes are aligned with the flow to minimize obstruction, and so do not actually constitute a ground plane as such. Nevertheless since they are all at ground potential, the effect should be to create a plane normal to the flow on which the voltage is zero. Different values of d were used, and the current and voltage recorded as the voltage was raised. The results are shown in Figure 5.1, in which $I/V \times 10^9$ is plotted against V. The solid lines are least square fits to the data for each

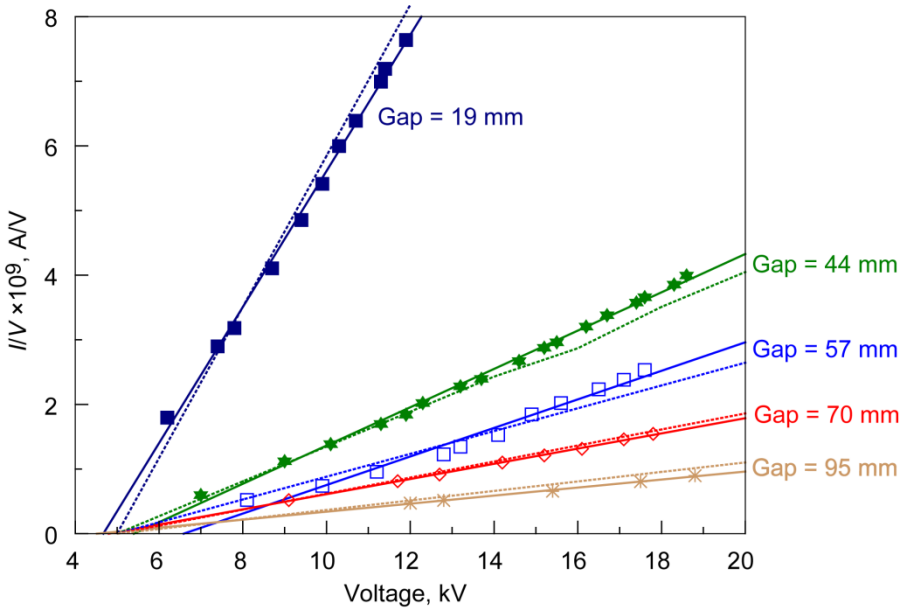

Figure 5.1.—Plot of *I*/*V* against *V* for three positive emitter electrodes, and four collector electrodes. Each emitter electrode has five sharpened tungsten points.

value of d, showing that in the ranges plotted, the current is proportional to $V(V–V_c)$. The critical voltage is seen to be about 5 kV. By finding the slopes of the lines, and plotting the log of the slope against the log of d, it was found that $K = 8.55\times10^{-11}$, and $(3\text{-}m) = 1.625$. With these values, plus $V_c = 5$ kV, $r = 2$ μm, and $\mu = 2.15\times10^{-4}$, I/V was calculated for each value of d, and is plotted in Figure 5.1 as the dashed lines. The agreement with the data is quite reasonable. If Equation (22c) is inserted into Equation (1), it is seen that the ion mobility cancels out. Thus the thrust depends only on voltage and the geometry. For a given voltage and gap size, thrust can be increased by reducing the critical voltage. This can be achieved by reducing the value of the point radius, r, or by using alternating voltage (Ref. 19). It should be noted that the points at the highest voltage for each gap represents the highest voltage for which the data does fit Equation (22c). The current becomes greater than the extrapolated straight line for higher voltages. However, this region is beyond the region where the higher values of θ are to be found. Note also that Cobine (Ref. 9) states that V_c is lower for positively charged emitters than it is for negatively charged emitters. For this reason, all experiments were run with positive emitters.

5.2 Relationship Between θ and Thrust

If Equation (22c) is used to calculate the current, given a voltage, the thrust can then be calculated from Equation (17). The power is given by the product of V and I, so θ can be determined. This has been done for $\mu = 2.15\times10^{-4}$ (air), and $r = 2$ μm, and the resulting curves of θ versus thrust, for four different gap sizes, are given in Figure 5.2. Note that this is not a general curve—the values of current are applicable only to the box lifter used (through the value of K), but the form of the curves should be general. It shows that θ is relatively insensitive to gap size at large values of thrust, where θ is relatively low. At low values of thrust, θ can equal or even exceed 20 N/kW. In this region, the gap size is important, and thrust increases with gap size at a constant θ = 20 N/kW.

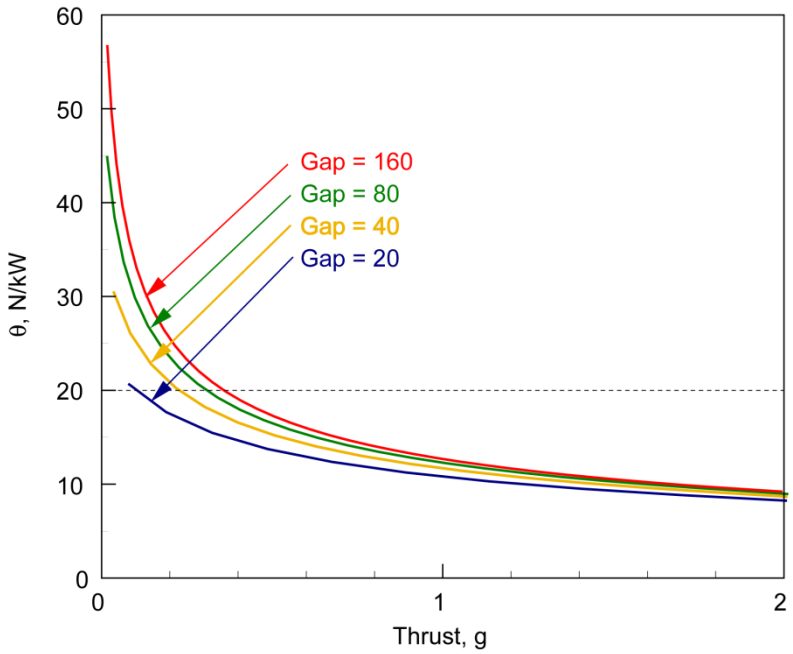

Figure 5.2.—θ versus thrust, as calculated using Equation (22c) for current, and Equation (17) for thrust, for each of four gap sizes.

6.0 Electric Field Calculations

In an effort to understand the variations in electrode separation, gap and type, the commercially available code Maxwell (Ref. 20) was exercised to evaluate field distributions at the emitter. The Maxwell code permits input of any desired geometry of emitter and collector, and finds the electrostatic field for this arrangement with an applied voltage. It does not allow for any discharge between the emitter and collector. In practice a problem arose since the electrode gaps are of the order of 50 mm, but the high field around the emitter only exists over a region of the order of 2×10^{-3} mm. This required a very fine grid near the emitter, and a coarse grid in the main gap so as to limit the number of points calculated. Even with this arrangement, results tended to be erratic, and with the exception of the results given below, are not given.

In an experiment not mentioned above, three emitter electrodes made of a series of razor blades placed edge to edge were used in the box lifter. The objective was to see whether a sharp two-dimensional electrode would perform better than wires, since the radius of the sharp edge would be much smaller than a wire. Also, since the effective emitting area would be larger than several pins, the resulting current might be greater than that of the pins, giving larger thrust. In fact no thrust was seen, and it was noticed that the discharge was confined to the ends of the electrodes, where a blue glow was seen. Clearly, the field was concentrated at the outside corner. The Maxwell code was used to study this, and the result, shown in Figure 6.1, confirms this. In the calculation for Figure 6.1, a razor blade is separated from a collector by 50 mm, and a voltage of 25 kV is applied. Only a small portion of the end of the razor blade is shown in Figure 6.1, corresponding to a length of about 0.25 mm. The razor blade is shown in grey. Contours of electric field are shown, with color used to indicate the field value. Away from the blade, the field strength is 5×10^5 V/m, indicated by the deep blue color. Note that the applied field, i.e., V/d is equal to 5×10^5 V/m. However, at the tip of the blade, there is a very concentrated region of field as high as 7×10^7 V/m: this region being shown in red. Thus it is not surprising that any discharge would be confined to the end of the blade.

Another calculation was made of the electric field at a junction between two razor blades, assuming that the blades are separated by a small gap of 5×10^{-2} mm. The result is shown in Figure 6.2, in which

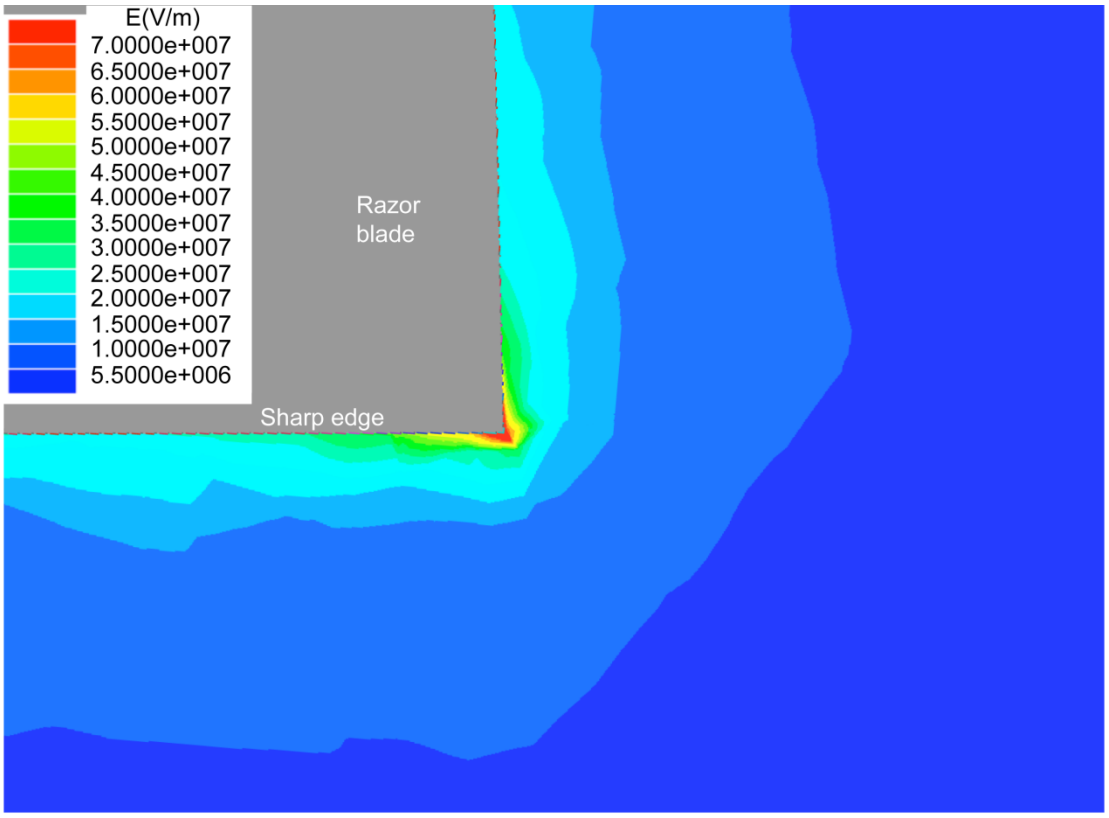

Figure 6.1.—The electric field distribution at the end of a row of razor blades. The length of blade showing in the picture is approximately 0.25 mm.

the blades are again in grey. It shows that in this case the field does not show any concentration at the junctions. Thus placing several razor blades in line is only going to give a high field concentration at the outside edges of the end blades, which is where the discharge will appear. This is consistent with what was seen experimentally.

Consequently, if a two-dimensional sharp electrode is to be used, some means of eliminating the field concentration at the outer ends is necessary. This is similar to the problem of generating a uniform field between two plane electrodes, for testing gas breakdown as a function of electric field. The solution for the plane electrodes is the Rogowski electrode (Ref. 9), in which the shape of the edge of the plate results in a decreasing field at large plate radii. The Rogowski electrode is a fairly complex shape, and rather than trying this, it was decided to calculate the field given by a simple ellipse at the end of a razor blade. The ellipse chosen had a semi major axis of 18.75 mm, and a semi minor axis of 6.25 mm. The same field and gap were used as above, and the result, shown in Figure 6.3, again with the highest field in red, and the blade in grey, shows that the field tapers off from the central region of the blade to the end of the blade. However, the highest field is only about 6×10^6 V/m, much lower than observed at the square end. Nevertheless, this geometry seemed to solve the problem of field concentration at the end of the electrode, and was tried experimentally, as will be described below.

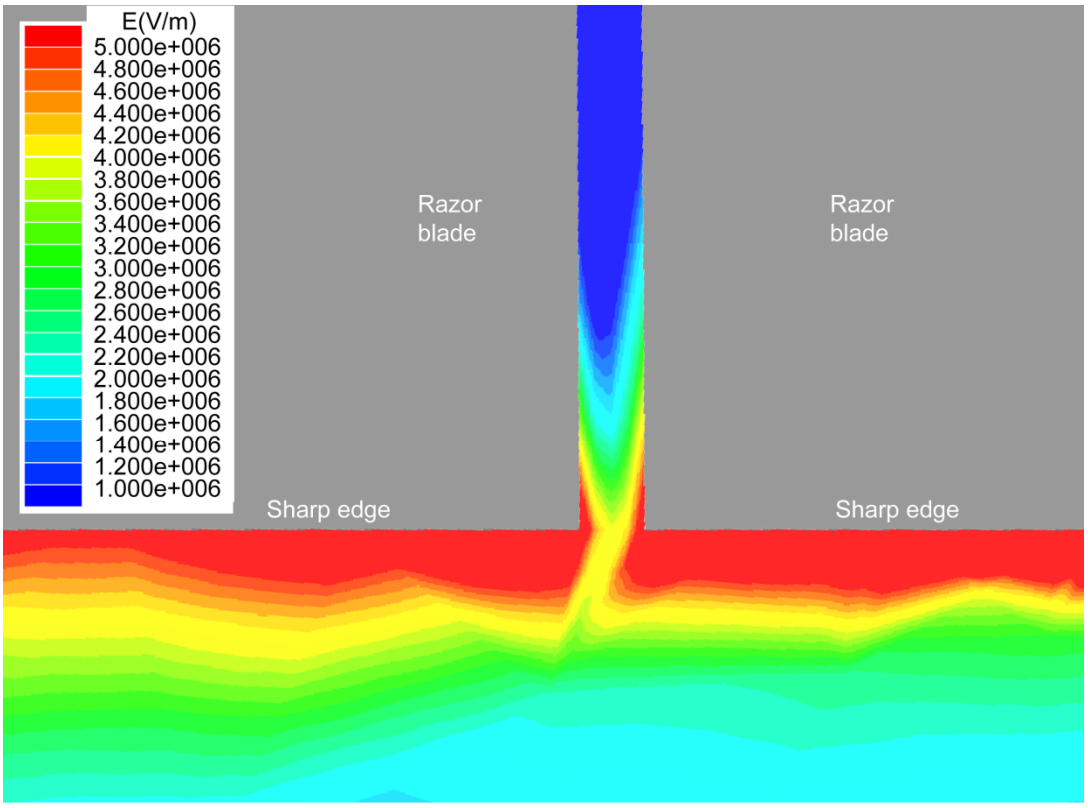

Figure 6.2.—The electric field at the junction between two razor blades. The gap between the two blades is 0.051 mm.

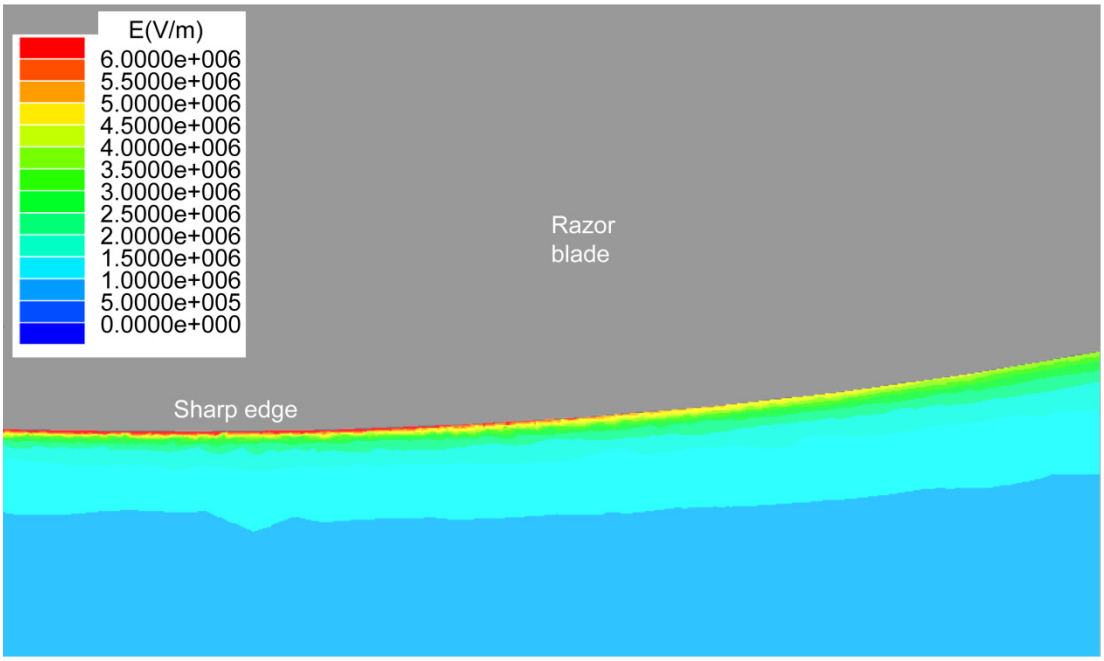

Figure 6.3.—The electric field distribution at a razor blade with an elliptically shaped end.

7.0 Experiments With Larger Rigs

7.1 The Apparatus

The experiments described above showed that to get good values of the thrust to power ratio, low fields were needed, resulting in low values of thrust. With the small box lifter used, thrust levels at low fields were in the region of tenths of a gram. The balance resolution was 0.1 g, and therefore the signal to noise ratio was not very good. Consequently, to get larger thrust levels, a larger box was built with foam-board end pieces, separated by foam-board side pieces, which were either 457 or 914 mm long, and 75 mm deep. In the first version, the electrodes were held in holes or slots in the end pieces. In the final version, a Lexan (SABIC Innovative Plastics) frame was made with the ground electrodes firmly attached to it. The frame measured 913 by 335 mm wide, and fitted inside the end pieces with fairly close tolerances. It could be moved vertically to permit different emitter to collector gap settings. The side and end-pieces were increased in height to 170 mm. A photograph of the rig is shown in Figure 7.1. Up to three emitter electrodes were used, each being made in the same manner as the electrode in Figure 4.1(a), using copper strips 0.4 mm thick, with pins soldered on. The emitter electrodes were either 490 or 950 mm long, with either eighteen pins for the smaller electrode, or thirty four pins for the larger electrode, with the spacing between pins equal to 25.4 mm. The emitter electrodes fitted into accurately machined slots in Lexan plates attached to the end-plates, and were joined electrically by a brass rod passing through the copper strips. Lexan spacers between the collector frame and the emitter electrode plates allowed accurate gap settings. The collector electrodes were made of streamlined aluminum tubing, purchased from a hobby store, having a thickness to chord ratio of 0.5. These were cut to the appropriate length, and provided with a screw at each end, which projected through the end pieces, and was fastened to a copper bus-bar, connected to ground. Figure 7.2 is a view from above the rig, looking down, and showing the emitter electrodes below, and the collector electrodes above. The ground bus-bar can also be seen in the lower right hand side of Figure 7.2. Connections from the ground bus-bar to ground, and the high voltage rod to the high voltage power supply were made with very fine wire, so as not to put any load onto the scale. A cross-section of the rig is given in Figure 7.3. The rig weighed 1,477 g.

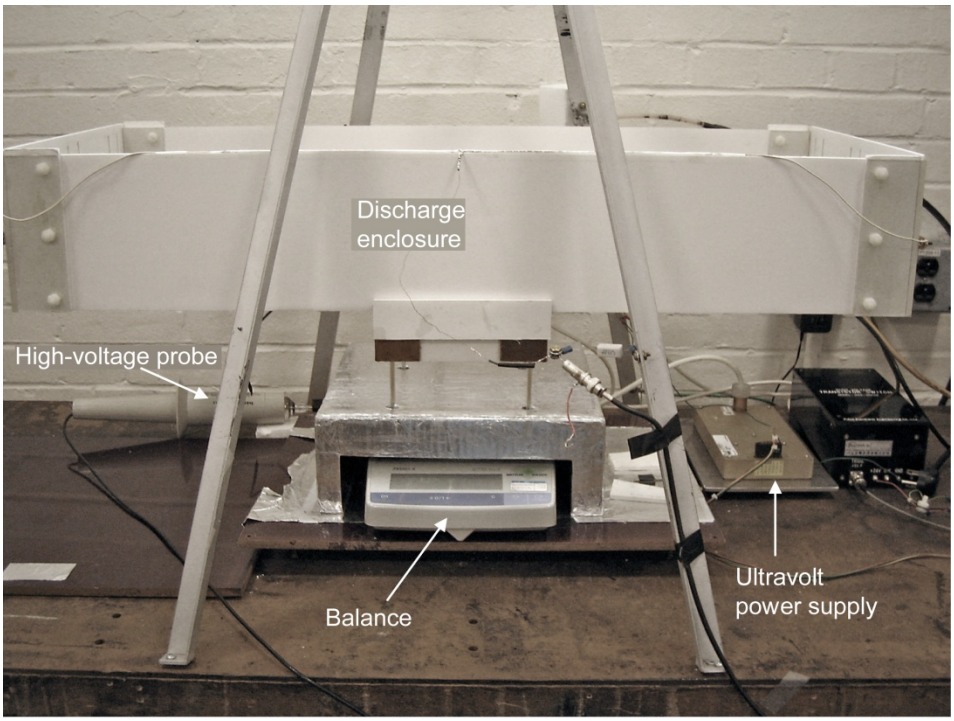

Figure 7.1.—Photograph of the larger discharge apparatus. The balance can be seen underneath the aluminum foil covered shield.

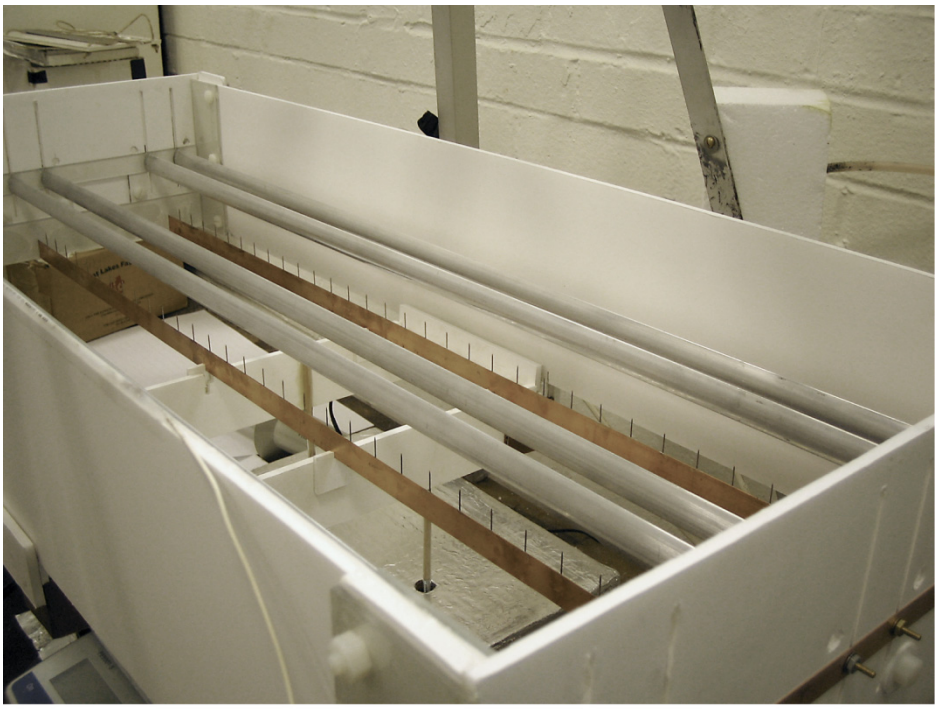

Figure 7.2.—Photograph looking down into the discharge apparatus. The aluminum rods are the collector electrodes (two to each emitter), and the copper strips with pins attached are the emitter electrodes.

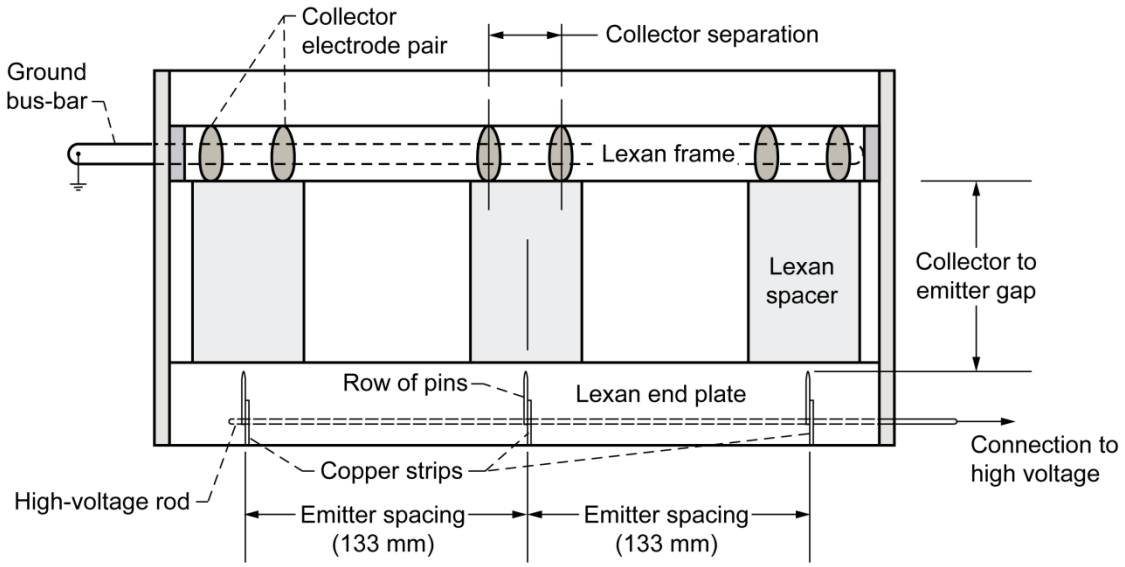

Figure 7.3.—Cross-sectional diagram of the corona discharge apparatus.

For nonpulsed experiments, the Glassman EQ30P40 Power Supply was used to provide high voltage. In order to measure the current, rather than using the built-in current meter, use was made of a connection provided by Glassman which gives a voltage proportional to current. This voltage signal was read on an Agilent 34401A digital voltmeter; the signal was calibrated using a precision resistor. This permitted greater accuracy in reading the values of current. For thrust measurements, the rig was mounted on a support stand, which had four vertical posts passing through a shield above the balance, and resting on the balance plate. This shield was wrapped in aluminum foil, which was connected to the electrical ground, so the balance was effectively sitting in a Faraday cage. This was to minimize any electrical pick-up from the discharge. Also

the emitter electrode, which was positively charged, was at the bottom of the rig, so that the ionic wind was directed upwards, and thrust appeared as an increase in the balance reading. This was done because earlier experiments with the ionic wind directed at the balance had showed spurious readings. Initially, the balance was the same Ohaus balance used above. This balance has a maximum load of 400 g, which is less than the weight of the rig. In order to bring readings into the balance range, an arm was mounted above the rig, supported on a knife edge, attached to the rig at one end, and with a counterweight on the other end. This was not entirely satisfactory, and later readings were made with a Mettler Model PB5001-S digital balance having a maximum loading of 5 kg, but still with a resolution of 0.1 g.

7.2 Emitter Comparison

It was decided to repeat experiments with different types of emitter electrodes, and measurements of thrust and current were made at various voltage levels. The emitters used were (1) a 450 mm long electrode with eighteen pins, (2) a 450 mm long wire, (3) a 900 mm long electrode made of 23 razor blades placed side-by side, with the end blades cut to an elliptical shape, and (4) a 864 mm long electrode fabricated from a single piece of stainless steel, 1 mm thick, with a razor sharp edge (Jewel Blade Company, Sheffield, England, Part No. FP1), also provided with elliptical ends, as shown in Figure 7.4. All tests were made at the same gap setting of 48 mm.

The results of this test are given in Figure 7.5, showing θ plotted against thrust. The two knife-edge emitters, although twice as long as the other two emitters, produced less thrust at maximum voltage, and for the razor blades, lower values of θ also. The Jewel blade did appear to give high values of θ at low thrusts, but, since these are at very low values of thrust, are probably inaccurate. The pin electrode is seen to be superior to the wire electrode, since it does generate values of θ greater than 20, at reasonably accurate thrust values, whereas the wire does not. Based on this, further efforts were concentrated on pin emitter electrodes.

7.3 Collector Studies

There are suggestions that multiple collector electrodes per emitter electrode might be preferable to a single collector. For example, the commercially available “Ionic Breeze” air circulator uses three ground electrodes and two emitter electrodes. Electrodes of large frontal area are claimed to be better than small ones (Ref. 7). Two tests were made to investigate this. In the first, a single thirty-four pin emitter electrode, and two collector electrodes separated by 44 mm were used. The emitter to collector gap was 25 mm, this low gap value being chosen to give good thrust values. Different collector electrodes were used, having chord lengths, *c*, of 6.4, 12.7, and 19 mm, respectively. These were a crude airfoil shape, with the same thickness to chord ratio, of about 0.5. Thus increasing the length (chord) also increased the thickness, i.e., frontal area. The results, plotted as θ versus *T* are given in Figure 7.6. These tests showed that, at least for values of θ near 20, the longer (and thicker) collector electrode was superior to the shorter ones. Even larger electrodes may be desirable.

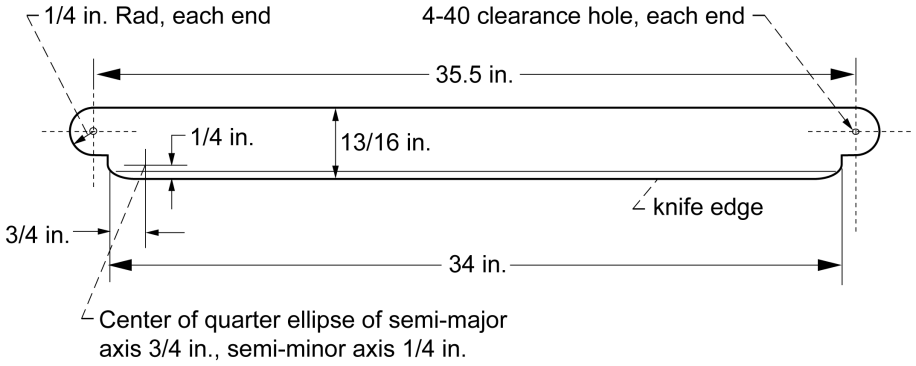

Figure 7.4.—Drawing of emitter electrode made from Jewel cutting strip (not to scale).

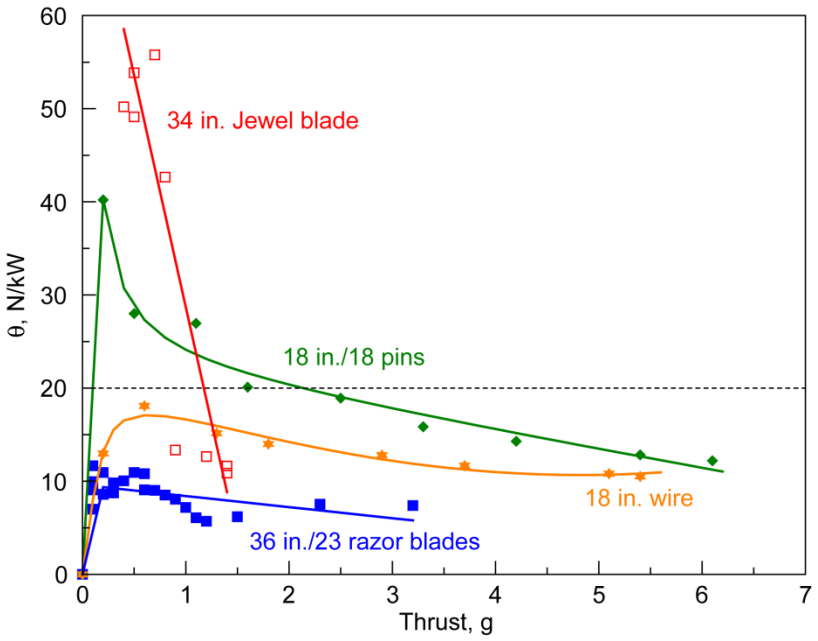

Figure 7.5.—θ versus thrust for four different emitter electrode configurations.

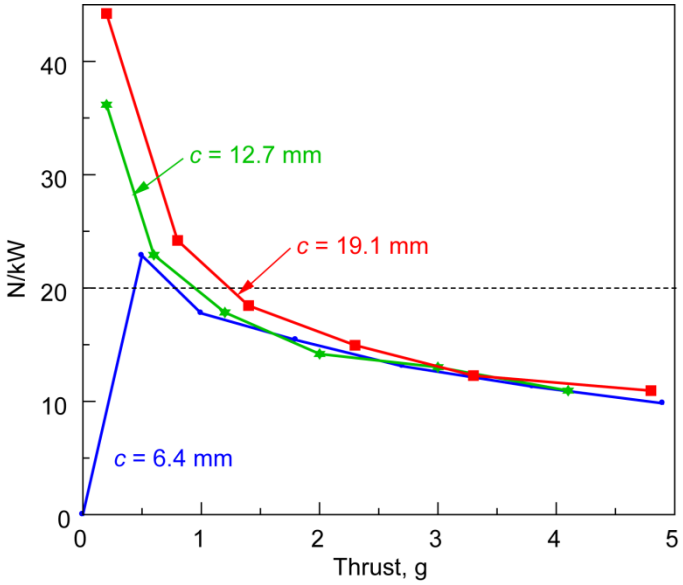

Figure 7.6.—θ versus thrust for three different collector chord lengths, *c*. A single emitter electrode with thirty four pins spaced 25 mm apart, and two collector electrodes, was used. The gap was 25 mm. The separation between the two collector electrodes was 44 mm.

In the second test, using only the 19 mm chord collector electrodes, since these had proved to be better in the first test, and again using a gap of 25 mm, the separation between collector electrodes was varied from zero, i.e., one electrode, to a maximum of 44 mm. Readings were made at four different voltages. The results, plotted as T versus collector separation, are given in Figure 7.7, and show that there is an optimum separation of about 33 mm, independent of applied voltage. It should be noted that this optimum separation was measured only at a gap of 25 mm, and might vary with gap size. In using multiple collectors, the emitter to collector gap, *d*, is defined as shown in Figure 7.3, i.e., as the distance between the tip of the pins, and a horizontal line tangent to the leading edge of the collector airfoils.

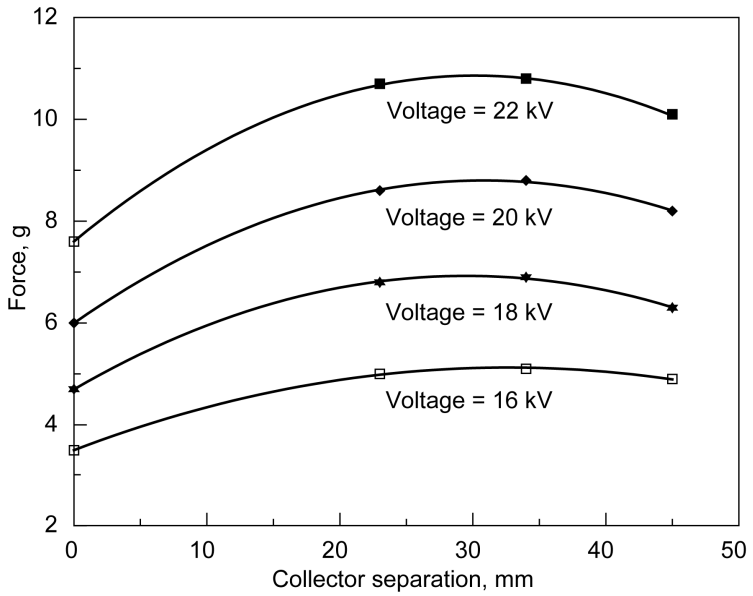

Figure 7.7.—The effect of varying the separation between two collector electrodes, in comparison with a single collector electrode (i.e., separation = zero).

7.4 Measurements of θ Versus *T*

Based on the above results, the final version of the test rig used a pair of 19 mm chord collector electrodes, separated by 33 mm, for each emitter electrode. To further increase the thrust, three emitter electrodes were used, separated by 133 mm. As stated above, the three pairs of collector electrodes were attached to Lexan plates at each end, forming a collector frame. The thrust was measured with the Mettler balance. This arrangement was used to make measurements of thrust and current at different voltages, for each of nine different gap settings. The results, plotted as θ versus *T*, are given in Figure 7.8, as the symbols, together with fits made with a statistical program. The fits were generally of the form:

$$\theta = a + b/T + c/T^2 + d \times T \tag{23}$$

although for the 105 mm gap, it was found that $c = 0$, and for the 75 mm gap, an extra term, $e \times T^2$ had to be added. It had been hoped that by plotting each of the constants versus the gap, and fitting the result, a model could be found which could be used to extrapolate the results to larger gaps. Unfortunately, although the individual fits of θ versus *T* were very good, the constants did not exhibit enough regularity that this procedure could be used with any confidence.

Constant voltage lines for 20, 25, and 30 kV are cross-plotted also. It can be seen that the trend is the same as that of the calculated results from Figure 5.2, namely that, at a constant value of θ, thrust increases with the gap size. Achieving this higher thrust requires higher voltage. At the highest voltage available, 30 kV, a gap size of 105 mm gave a value of θ equal to 20 N/kW, with a thrust of 13.1 g. Note that at the lower gaps, the discharge arcs at voltages below 30 kV, so that this is a limit on how much voltage can be applied to a given gap. For a given desired value of θ, using a voltage just below the arcing value, and the corresponding gap will give the maximum thrust available from that rig. This point will be revisited below.

In Figure 7.9, current versus voltage curves are given for each of the nine gaps used in obtaining the data of Figure 7.8. The symbols are the data points, and the lines are statistically-fitted curves. The fits were of the form:

$$I = a + b \times V + c \times V^2 + d \times V^3 + e \times V^4 \tag{24}$$

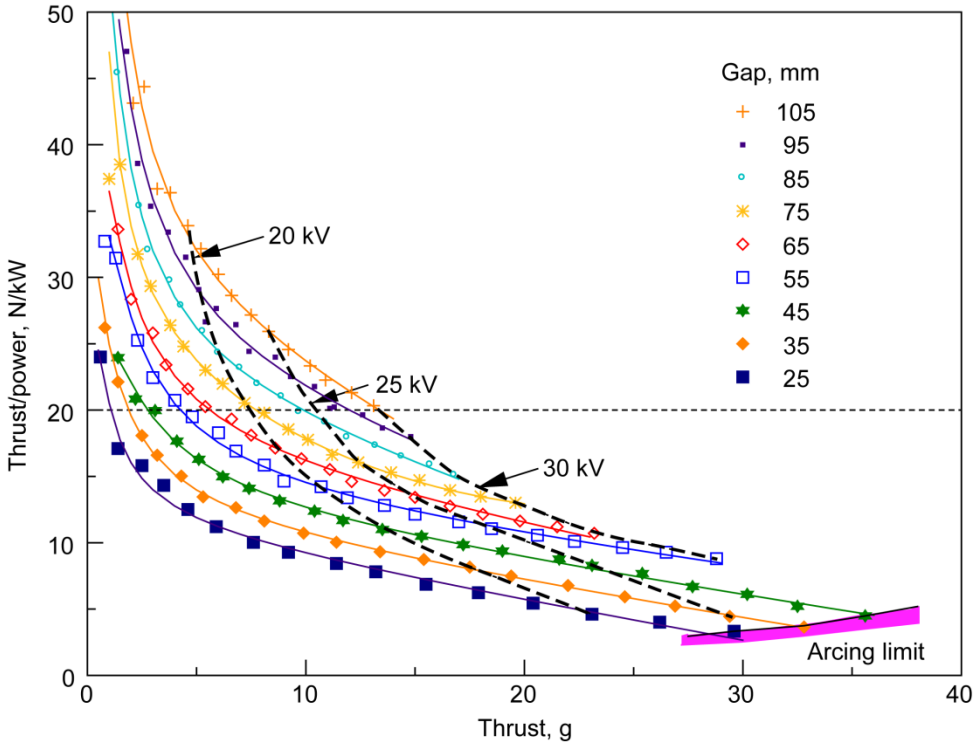

Figure 7.8.—Thrust divided by power versus thrust as a function of gap size and voltage for the large rig with three 450 mm long pin emitter electrodes, as seen in Figure 7.2.

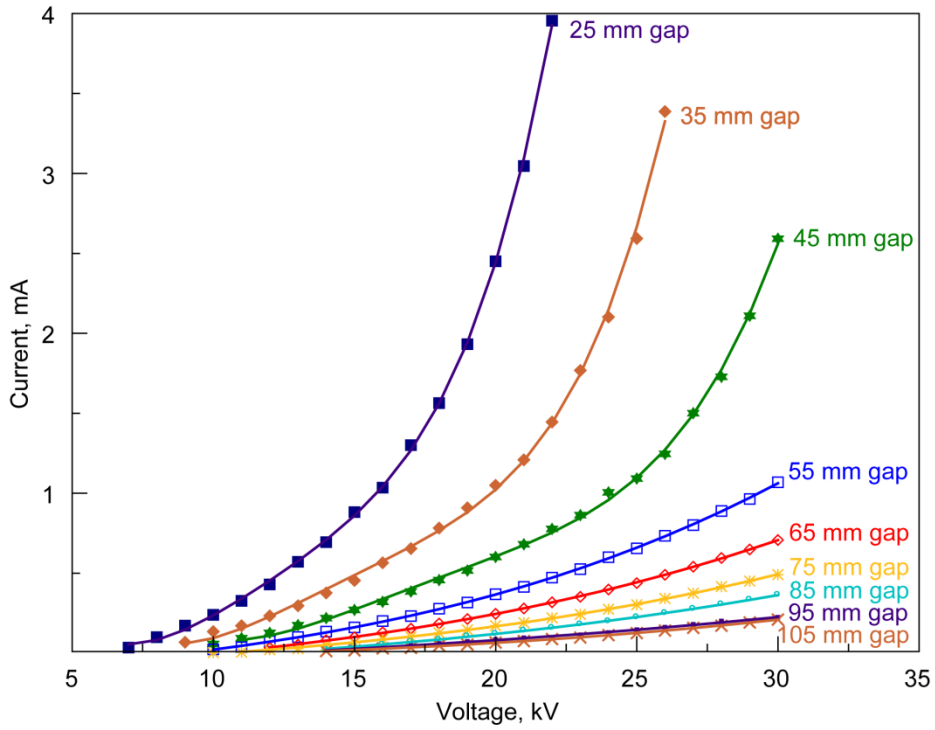

Figure 7.9.—Current versus voltage for the discharges used to obtain the data of Figure 7.8.

The values of the constants are given in Table 3, in which the values listed give the current in milliamps when the voltage is input in kilovolts.

TABLE 3.—VALUES OF THE CONSTANTS IN EQUATION (16) WHICH GIVE THE CURRENT AS A FUNCTION OF VOLTAGE FOR DIFFERENT GAPS

d, mm	*a*	*b*	*c*	*d*	*e*
25	2.9552	–1.1141	0.1489	–0.008214	0.0001745
35	3.9561	–1.2318	0.1365	–0.006270	0.0001080
45	4.0493	–1.0420	0.09619	–0.003698	0.00005314
55	–0.1460	0.01393	----------	0.00002927	----------
65	–0.1418	0.01223	---------	0.00001786	----------
75	–0.0978	0.00815	---------	0.00001285	---------
85	–0.1108	0.00817	---------	0.00000849	---------
95	–0.0977	0.00751	---------	0.00000363	---------
105	–0.0553	0.00374	---------	0.00000566	---------

It will be seen that two different models fit the data; one for gaps of 45 mm and below, and one for gaps above 45 mm. Neither of these models is in agreement with Equation (22), which has only a linear term plus a quadratic term, and no constant.

8.0 Experiments With Pulsed Excitation

8.1 Background

It has been proposed previously (Refs. 1, 3, 15, and 21) that pulsed excitation may give better results than direct current excitation. Indeed, Naudin (Ref. 15) claimed to have achieved a reduction in power of a factor of 3 to generate the same thrust at 100 Hz as via direct excitation. Lower frequencies produced less of an improvement. One possible factor in this improvement is that there is a reduction in V_c for pulsed excitation (Ref. 19). To be precise, this is for AC voltages, with both a positive and a negative half-cycle. The remaining ion cloud from one half-cycle is attracted back to the emitter on the voltage reversal. This increases the field at the surface of the emitter, so that emission can begin at a lower voltage than in the steady case. This effect will be more important at low voltages than at high voltages. In the case of a voltage that is pulsed only positively or negatively, there is a critical pulse length for which the pulsing should result in a change. If the pulse length is long, the ions can cross the gap completely, and the situation is little different from a steady voltage. However, at a certain pulse length, the ions can no longer cross the gap during the pulse length, and will remain in the gap afterwards. This critical pulse length is easily calculated. The ion cloud travels at the ion velocity, given above as $v_i = \mu E$, so that it takes a time t_c to cross the gap, d, where:

$$t_c = d/v_i = d/\mu E = d^2/\mu \tag{25}$$

For the smallest gap used, namely 25 mm, at 20 kV excitation, $t_c = 0.16$ msecs, and at the largest gap used, 105 mm, at 25 kV excitation $t_c = 2.7$ msecs. If the pulse is repeated after a delay of the same magnitude, these times correspond to 3 kHz, and 200 Hz, respectively. What happens when the ion cloud does remain in the gap is not clear, since there will be no force on it once the field is removed.

It was decided to make experiments to try to examine the effect of pulsed excitation. In particular, there was motivation to try a concept from laser technology, called double discharge (Ref. 22). This concept is that the optimum electric field for the objective (i.e., laser action, or thrust production) may be very different from that required to produce a significant degree of ionization. Consequently, a short, high voltage pulse is used to generate electrons, and then a lower field, optimum for the application, is applied for a longer time. It has been shown above that, for a corona discharge, a low field is optimum for

efficient thrust generation, but results in low thrust due to the resulting low electron concentration. Thus the double discharge technique might be useful for corona discharge thrust generation.

8.2 The Apparatus

Initial attempts were made to create a square wave voltage pulse using an Ultravolt 25C24 P125 High Voltage power supply. This power supply permits control of the output voltage by means of a 0 to 5 V control signal. It was thought then, that by applying a repetitive square wave control signal, the output voltage, which would be applied to the discharge, would also be a square wave. This did not prove to be the case; the unit having an output capacitance, which when combined with the very large impedance of the discharge (typically over one gigohm), resulted in a decay time of tens of milliseconds, meant that the voltage did not decay much between pulses. At 100 Hz, the result was that the applied voltage was not much different from a DC voltage, and no increase of θ was seen.

At this point, a high voltage switch was made available for these experiments. The switch was a Pulse Voltage Engineering Co. Ltd. High Voltage Transistor Switch, model HVS-36K20. This unit can withstand 36 kV, until a 5 V control signal is applied from an external trigger generator, when the switch is electronically opened. When open, the switch has an impedance of 120 Ω. The unit requires an external DC voltage of 24 V, which was provided by a Tektronix PS280 DC power supply. However, the high voltage switch has a duty cycle which is limited to 0.01 or less. Thus at 100 Hz, the maximum pulse length is only 100 μsecs long. Thus this pulse did not seem of sufficient duration to provide the sole excitation, but did seem suitable for the high voltage pulse of a double discharge arrangement. The apparatus is shown diagrammatically in Figure 8.1. The Glassman EQ30P40 high voltage power supply was used to provide the high voltage pulse, via the high voltage transistor switch. The lower voltage DC voltage was provided by the Ultravolt power supply, with a DC voltage on the control input. Blocking diodes were provided so that the two power supplies did not feed into each other.

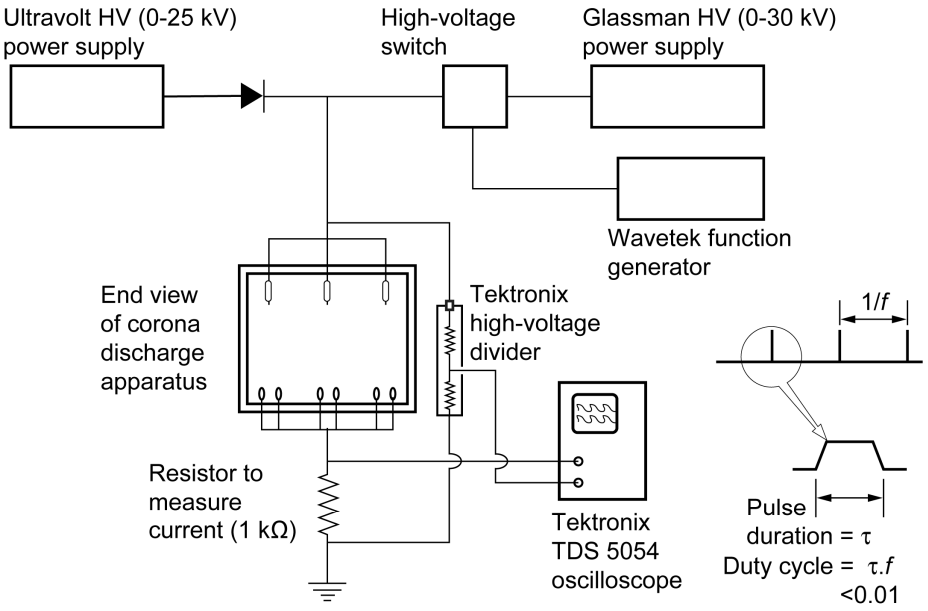

Figure 8.1.—Schematic diagram of the apparatus for powering the corona discharge with pulsed and DC voltage.

8.3 Experiments

8.3.1 Optimum Pulse Duration

An experiment was run with the objective of assessing the optimum pulse duration. For this experiment, the Ultravolt power supply was set at 10 kV, and the Glassman power supply at 20 kV. A Wavetek Model 166 signal generator provided a 5 V control signal to the high voltage switch. The frequency, *f*, and duration, τ, of this signal could be set independently. The discharge rig was the version described in Section 7.4, with the gap set at 35 mm. Thrust was measured as a function of frequency, with the result shown in Figure 8.2. For a pulse duration of 10 μsecs, the maximum frequency was 1 kHz because of the duty cycle limitation. The results are shown as the black data points and connecting line in Figure 8.2. It is seen that at the lowest frequency used, the thrust is equal to the DC value for 10 kV excitation, in other words, the pulses are adding nothing to the thrust, which comes entirely from the DC excitation. As the pulse frequency increases, the thrust also increases monotonically, until the maximum value of frequency of 1 kHz is reached. Next, this experiment was repeated without the DC excitation voltage. The results are the red data points and connecting line in Figure 8.2. At 30 Hz frequency, the thrust is zero, but above 300 Hz, it is identical to the data with 10 kV bias. Thus above 300 Hz, the DC bias is contributing nothing.

Switching to a 1 μsec duration pulse, without any steady bias voltage, gave the blue points and connecting line in Figure 8.2. Starting at 100 Hz, and continuing up to 1 kHz, this data overlaps the data for a 10 μsec duration pulse. However this curve was continued up to 30 kHz. For 5 kHz and higher frequencies, the thrust was equal to the thrust for a DC excitation of 20 kV. Thus at the high frequencies, the pulses seem to be equivalent to DC excitation. The experiment was repeated for a 100 nsec pulse duration, and a 40 nsec pulse, the shortest that could be generated by the Wavetek signal generator. The results are the orange and green data, respectively. These pulses gave less thrust than did the 1 μsec pulse.

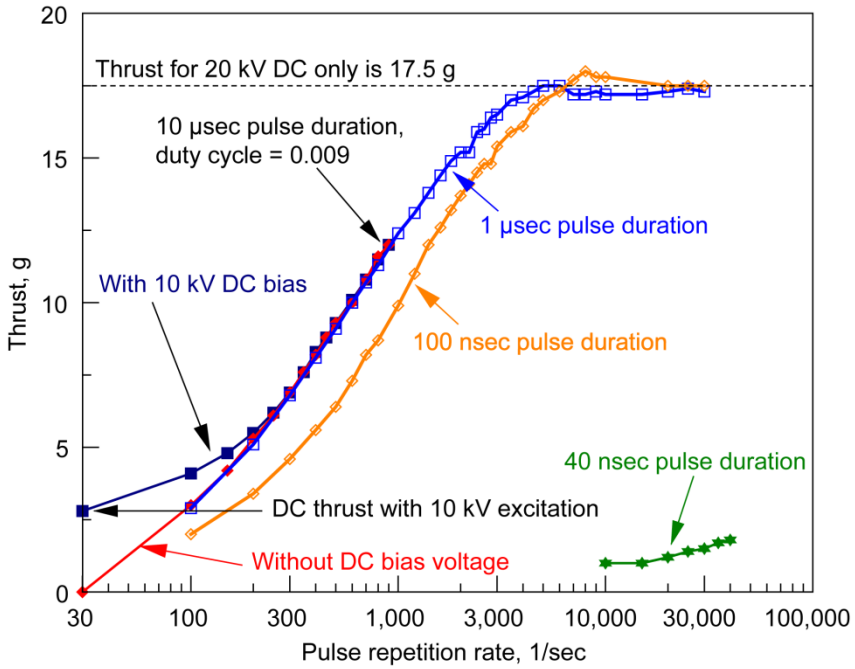

Figure 8.2.—The effect of varying the pulse duration and frequency on the observed thrust. The gap is 35 mm, the pulse durations are 10, 1, 0.1, 0.04 μsec, and the pulse voltage is 20 kV.

Based on these experiments, it would appear that a 1 μsec pulse is optimum. It gives the same thrust as a 10 μsec pulse, but can go to higher frequencies (because of the duty cycle limitation of the high voltage switch). However it gives more thrust than the shorter pulses. Based on this conclusion, the pulse duration was set at 1 μsec for all further experiments.

8.3.2 Power Measurement

Obviously to determine θ, the power is needed as well as the thrust. For pulsed excitation, the instantaneous voltage and current will be needed, whose product will give the instantaneous power, which can be averaged over one or more complete cycles to provide the average power. The current was measured by inserting a 1 kΩ resistor in the ground return line, and displaying the voltage at the nonground end on a Tektronix TDS 5054 Digital Phosphor Oscilloscope, as shown in Figure 8.1. The voltage was measured using a Tektronix P6015A High Voltage Divider, which has a frequency response of 75 MHz, and a resistance of 100 MΩ, attached to the high voltage side of the discharge. The discharge gap was again 35 mm. Some oscillograms are shown in Figure 8.3(a) for a frequency of 200 Hz, and in Figure 8.3(b) for a frequency of 1 kHz, using pulsed excitation only, i.e., no DC bias, with the Glassman power supply set to 20 kV. It is clear that the voltage and current last much longer than the 1 μsec on-time of the high voltage switch. Indeed, at a frequency of 1 kHz, the voltage is almost flat, i.e., equivalent to DC. This would seem to suggest that either the discharge, or the high voltage switch, has significant capacitance.

Following these tests, the gap was reset to 55 mm, and the Glassman Power Supply voltage raised to 30 kV, in order to generate more thrust, in a region where θ might be higher. As above, current and voltage were recorded on the digital oscilloscope. The results of current and voltage were stored, then transferred to an Microsoft Excel (Microsoft Corporation) file on a computer. At each reading, power was calculated by multiplying voltage and current, and the average found over an integer number of cycles. The value of θ followed by dividing the thrust by the average power. This was repeated for several values of frequency between 200 Hz and 1.8 kHz. The results are the blue line plotted in Figure 8.4, as θ versus thrust. Also shown, as the red line, are the values obtained at the same gap setting in the DC tests (Fig. 7.8). For the pulsed excitation, this figure seems to show θ decreasing linearly as the thrust increases, with a value of θ = 20 N/kW being achieved at 800 Hz, with 18 g of thrust. This is a significant improvement over the DC result at the same gap setting of θ = 20 N/kW at less than 5 g of thrust. However, there is some question as to whether these results are valid. In looking at the oscillogram of Figure 8.3(b), it is seen that there is considerable ringing noise on the current trace. Some of this is due to pick-up from the high voltage switch. This gets worse as the frequency is raised. Thus the current reading is uncertain at best.

An alternate way to calculate the power going into the discharge is to assess the energy change on each cycle, assuming that there is indeed capacitance in the circuit. If the high voltage switch has capacitance C_{hvs}, and the discharge apparatus has capacitance C, for a total capacitance ($C + C_{hvs}$), which is charged to a voltage V_0 when the switch closes, and decays to a voltage V_f just before the switch opens, then the energy flowing through the switch each cycle, E, is:

$$E = 0.5\left(C + C_{hvs}\right)\left(V_0^2 - V_f^2\right) \tag{26}$$

If R_{total} is the resistance through which the energy is dissipating, which consists of the resistance of the corona discharge R, and the resistance of the high voltage divider R_{vd}, in parallel, i.e.,

$$R_{\text{total}} = \left(1/R_{vd} + 1/R\right)^{-1} \tag{27}$$

(a)

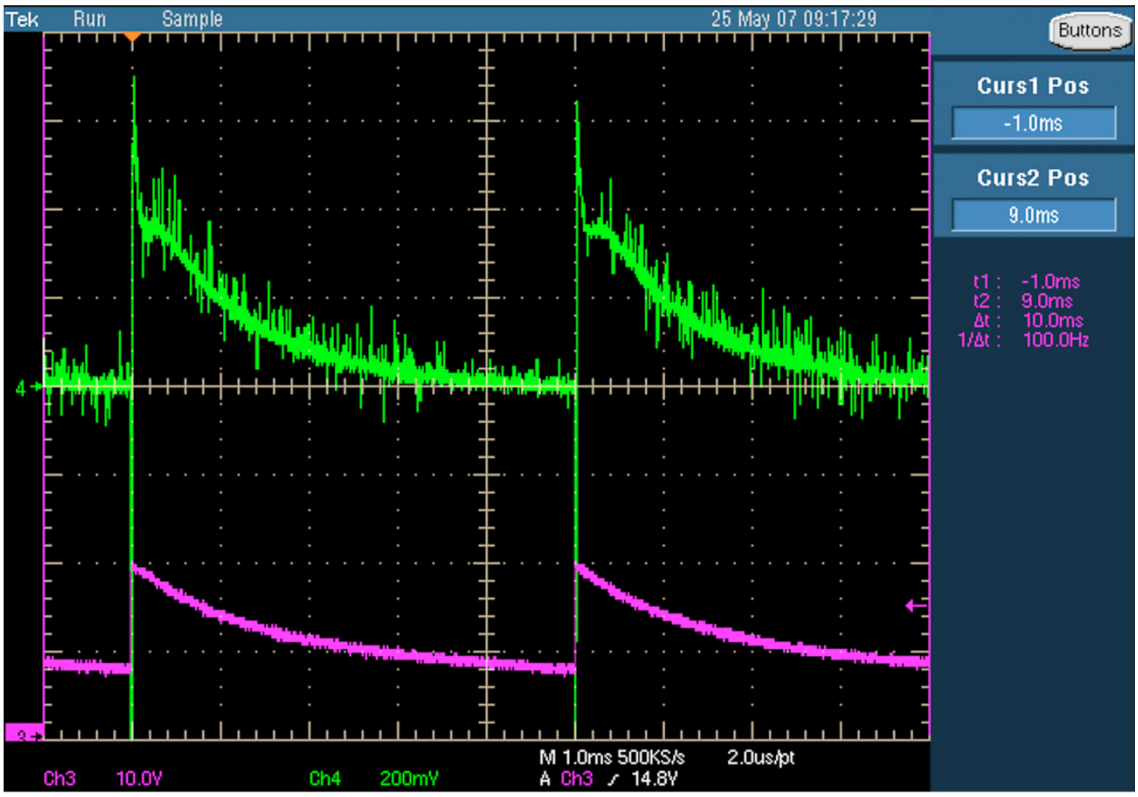

(b)

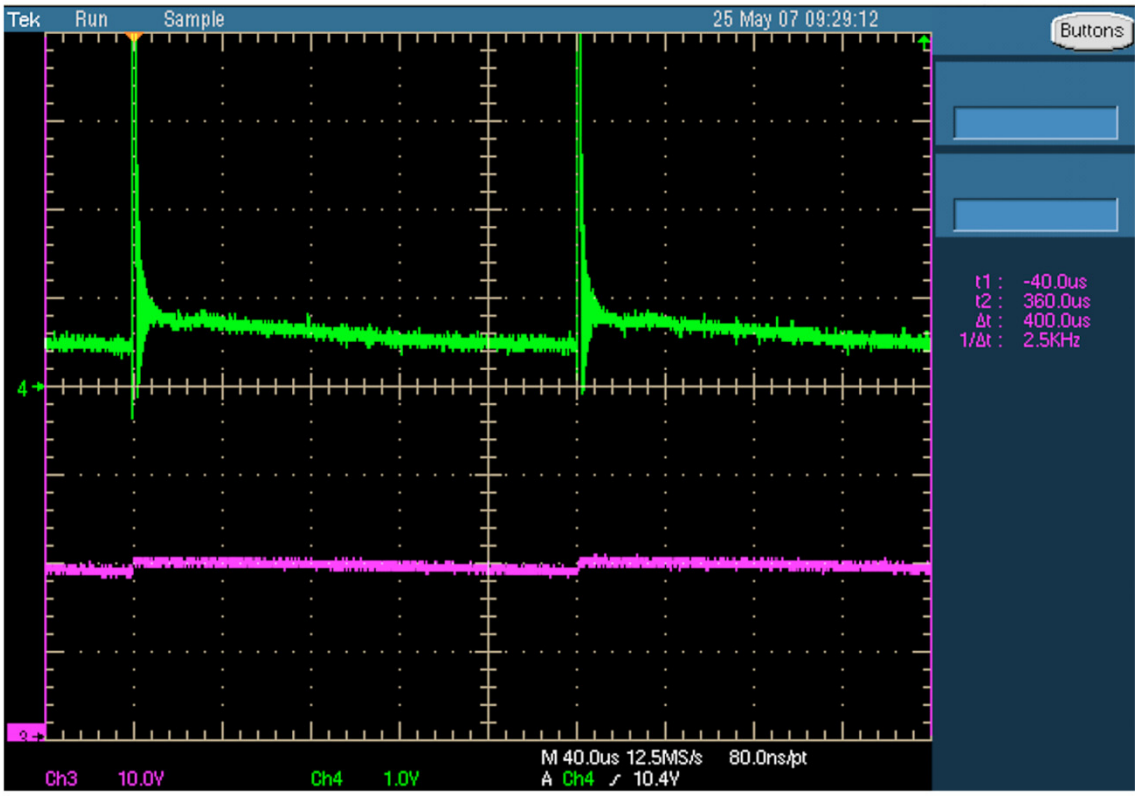

Figure 8.3.—Oscillograms of corona discharge voltage and current versus time. The lower trace is voltage, with a sensitivity of 10 kV/division, and the upper trace is current, with a sensitivity of (a) 0.2 mA/division, at a frequency = 200 Hz, and (b) 1 mA/division at a frequency = 1 kHz.

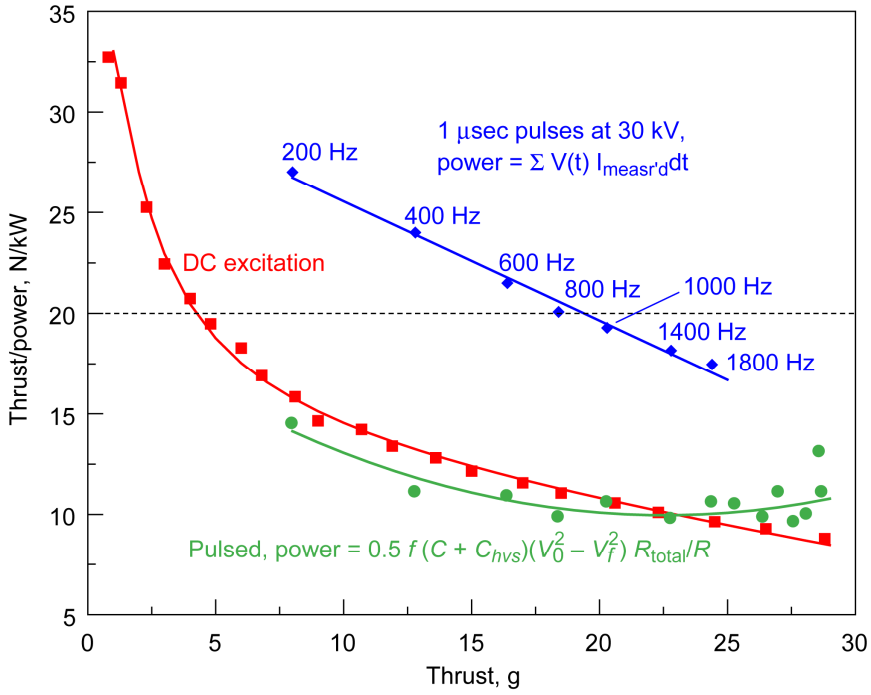

Figure 8.4.—Thrust divided by power at a gap size of 55 mm.

then the power flowing through the corona discharge, P, is:

$$P = 0.5\, f\left(C + C_{hvs}\right)\left(V_0^2 - V_f^2\right)\ R_{\text{total}} / R \tag{28}$$

which provides another calculation of the average power, independent of the current measurement. However, it does require knowledge of the capacitances of the switch and the discharge, and the resistance of the discharge. The capacitance of the switch is fairly easily determined by disconnecting the corona discharge, and measuring the voltage decay over one cycle. The resistance is then that of the high voltage divider only, and the capacitance is only that of the switch, and its value follows from the equation for an exponential decay as:

$$C_{hvs} = 1/\left(R_{vd}\, f \ln\left(V_f / V_0\right)\right) \tag{29}$$

Six measurements were performed, at three frequencies, namely 200, 600, and 1,000 Hz, and 2 V, 20 and 30 kV. The resulting average value of the switch capacitance was 67 pfarads. For the rig itself, a Sencore LC53 Capacitance-Inductor Analyzer was used to measure the capacitance between the high voltage connection and ground. The results are given in Table 4.

TABLE 4.—THE CAPACITANCE OF THE DISCHARGE RIG, C, AS A FUNCTION OF THE ELECTRODE GAP, d

Gap, d, mm	25	35	45	55	65	75	85	95	105
Capacitance, C, pf	59	56	53	51	49	47	46	45	44

These values are plotted in Figure 8.5. The capacitance does not seem to be inversely proportional to d, as might be expected, but does at least decrease monotonically as d increases.

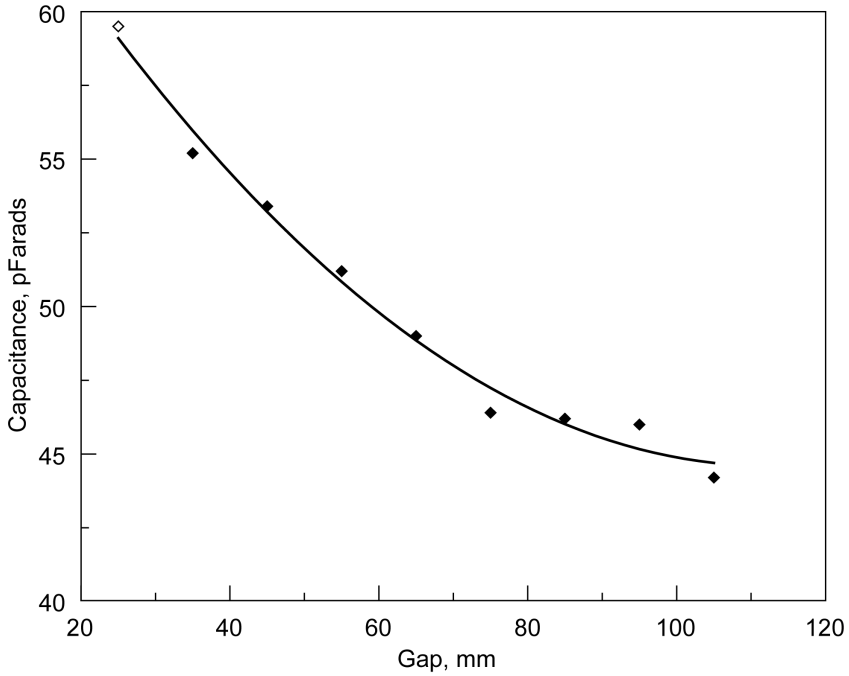

Figure 8.5.—The capacitance of the emitter to collector apparatus, as a function of the gap size.

With the capacitances determined, R is the only remaining unknown in Equation (28). By determining V_f and V_0 in runs with both the high voltage divider in place and the corona discharge, R_{total} can be evaluated from the voltage decay rate by assuming that R does not change much in one cycle. i.e.,

$$R_{\text{total}} = 1/\left(\left(C + C_{\text{stray}}\right) f \ln\left(V/V_0\right)\right) \tag{30}$$

With R_{total} known, R can be obtained from Equation (27), and hence the power evaluated from Equation (28). The difficulty with this procedure is that R is not constant during a pulsed discharge, since the voltage is dropping continuously, after the switch is opened. In Figure 8.6, the DC corona discharge data of Figure 7.9 are replotted as resistance against voltage, with the gap size as a parameter. It will be seen that the discharge has a resistance of 100 MΩ, i.e., the same as that of the voltage divider, for d = 85 mm at an excitation voltage of 30 kV. Thus, roughly, a gap of 85 mm represents a border between the pulsed voltage decay being determined by the fixed resistor of the voltage divider, and the changing resistance of the discharge as the voltage drops. At higher gaps, and lower voltages, the decay will be more like that for a fixed resistor, and vice-versa. The procedure will be more accurate, the more the decay is like that for a fixed resistor.

8.4 Experimental Results

In Figure 8.4, values of θ calculated with the power being determined by the energy change of the stray capacitance are given as the green points as well as the values given by calculating the power from the product of current and voltage (i.e., the blue points). It can be seen that the values calculated from the capacitance are very close to the DC values, except possibly at high thrusts (i.e., high frequency). This might suggest that there is no advantage in pulsing, in disagreement with the results with power calculated from the voltage-current product, or that there might be an effect at high frequency. All the results in Figure 8.4 are for a gap of 55 mm. It therefore seemed worthwhile exploring other gap sizes, using the capacitance method for calculating power. The results are shown in Figure 8.7, again with θ

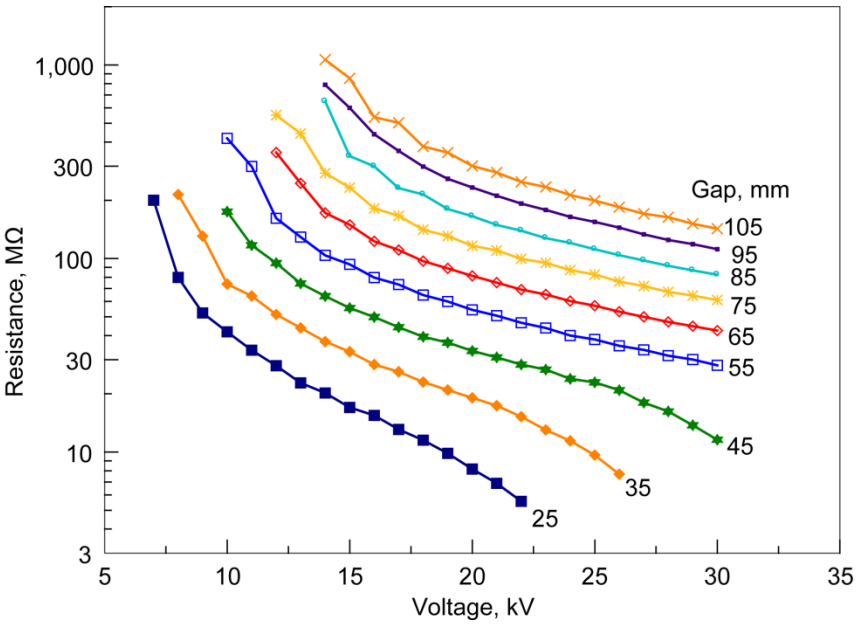

Figure 8.6.—The resistance of the corona discharge as a function of gap and voltage.

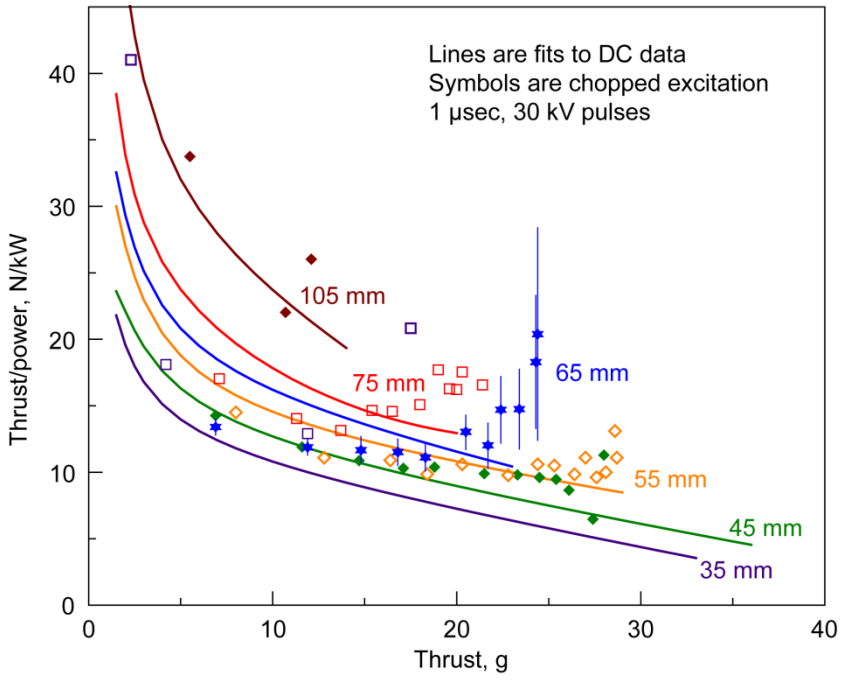

Figure 8.7.—Thrust divided by power versus thrust, with the power calculated from the capacitance energy drop per cycle.

plotted against thrust. The solid lines without data points are the DC results from Figure 7.8. The results for a gap of 65 mm (the blue points) are particularly interesting as they indicate that it may be possible to achieve θ = 20 N/kW at a thrust of about 25 g. Note however, that there is significant uncertainty in these results, as indicated by the vertical lines. This is because V_f and V_0 are not very different as the frequency increases, so the situation is one of subtracting two large numbers to get a small result, which is well known to be fraught with error. If indeed there is an advantage of pulsing at high frequency, this result seems rather surprising as the voltage at high frequency is almost constant, so it would seem that this situation should not differ from the DC result.

8.5 Comments on Pulsed Excitation

From the results shown here, it cannot be definitely concluded whether or not there is an increase in θ at a fixed value of thrust due to using pulsed excitation. The results when the power into the discharge was calculated from the voltage-current product appear most promising, but suffer from doubt as to whether the current measurement was accurate. The results using the change in energy of the stray capacitance to calculate the discharge power do not show any improvement at low frequencies, and require knowledge of the stray capacitances, which may not have been determined very well. Also needed is the value of the discharge resistance, which was obtained from the rate of voltage decay assuming that this resistance is constant, which it is not. Clearly, this is a topic which needs further research.

It should also be pointed out that these experiments were not a true test of the double discharge technique, as the supposedly short duration pulse was actually stretched out due to the long voltage decay time caused by the combination of stray capacitance and high resistance of the discharge.

9.0 Extrapolation of the Results

It is of interest to estimate what is the maximum thrust that this apparatus could produce, and hence what scaling-up in size is required to generate the 500 N of thrust for Helios, assuming that θ = 20 N/kW. From Figure 7.8 it can be seen that as one moves along the line of constant θ = 20, from left to right, the thrust is increasing, and at the same time, so is the gap, and the voltage required. In Figure 9.1, values of thrust for each gap size (interpolated as necessary) at θ = 20 N/kW are plotted against the electrode gap size. Also shown is a cubic fit to the data, which fits well except for the point at a gap of 105 mm. If the cubic fit is correct, the maximum thrust would be about 45 g, at a gap of 250 mm. However, it is probable that this value could not be achieved, as the corona discharge would develop into an arc. In Figure 9.2 the voltage required to achieve θ = 20 N/kW (the pink points) is plotted versus the gap size, together with a fit (the black line). Also plotted are the few points at which the discharge did arc (the red diamonds). The dashed red line is an extrapolation of these points to large gap size, showing that it meets the voltage required for θ = 20 N/kW at a gap of 200 mm, and a voltage of slightly less than 80 kV (i.e., the black point). Returning to Figure 9.1, a voltage of 80 kV at a gap of 200 mm would give a thrust of about 37 g. This then is the maximum practical thrust achievable with the present rig, unless pulsing the excitation voltage would increase the thrust at the same value of θ. Roughly then, the thrust achievable might be about 50 g, or 0.5 N. The frontal area of the rig is 0.33 m^2, so that with a thrust of 0.5 N, the value of ϕ would be 1.5 N/m^2, a factor of three lower than the maximum value achieved by Christenson and Moller (Ref. 3). However, by staging three units in-line, the thrust should be tripled at the same area, giving ϕ = 4.5 N/m^2. This is still below the goal of 20 N/m^2, so that unless significant improvements can be made, the technology does not seem very practical. To meet the thrust needed for Helios, a scale-up of a factor of 1,000 in thrust is needed. The thrust needed for the Lockheed High Altitude Airship (HAA) (Ref. 5) application is not obvious, but might be of the order of 5,000 N, for a scale-up in size of 10,000. Moreover, since more surface area is available on the HAA, this might be more practical. However, this airship will fly at high altitude, where the ionic wind is undoubtedly reduced due to the lower density.

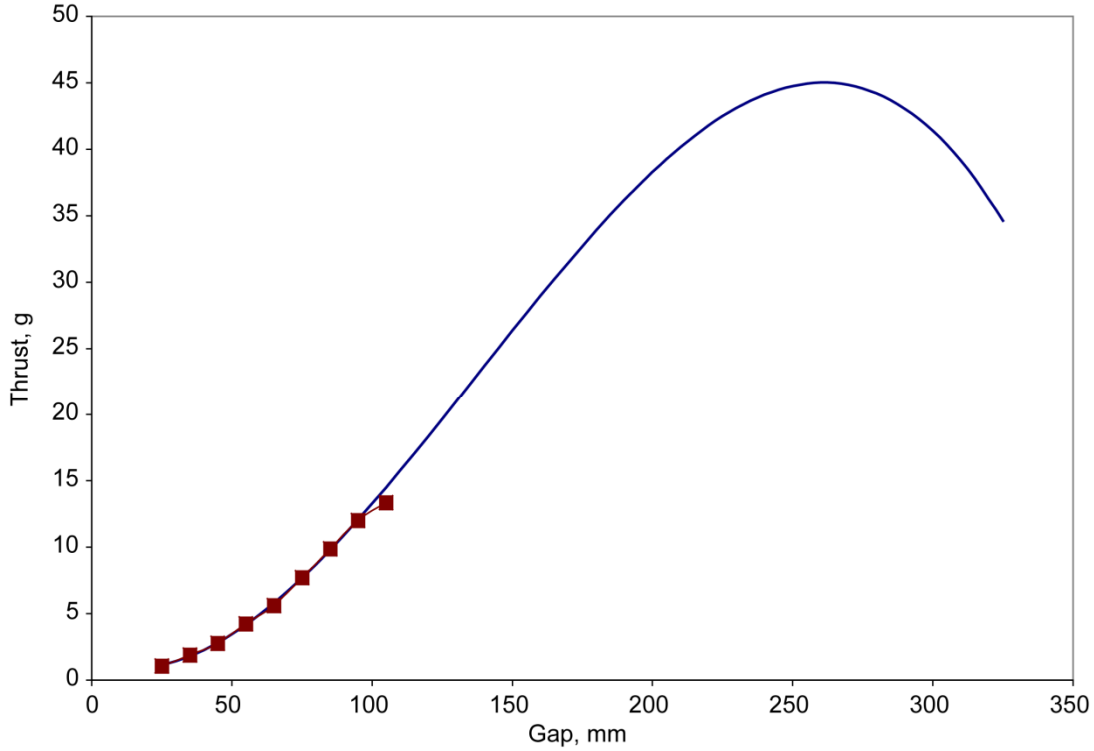

Figure 9.1.—Thrust versus electrode gap at θ = 20 N/kW.

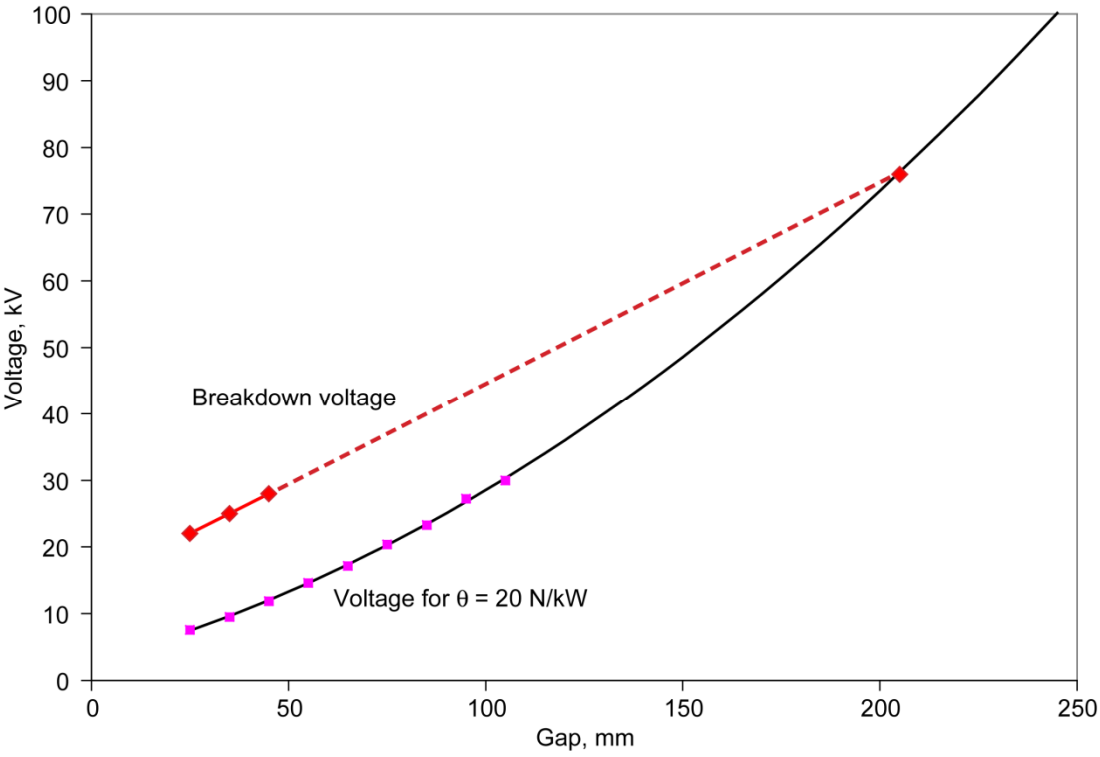

Figure 9.2.—Voltage versus electrode gap at θ = 20 N/kW.

10.0 Discussion

The goals of the program, namely, $\theta = 20$ N/kW at $\phi = 20$ N/m^2, were not realized, although the desired thrust per unit power was achieved. However, achieving the thrust per unit power meant that a very low level of thrust was developed. A parametric study of the thrust per unit power versus thrust (Fig. 7.8) was made with electrode gap and voltage as parameters, and even though this pointed the way to improvement, the extrapolation was not encouraging. This seems to be inherent in the physics of the corona discharge, and little can be done about it. Efforts to increase current at a given electric field strength (i.e., brush electrodes, and razor blade electrodes) only seemed to reduce the thrust per unit power. However, more work on the emitter may be in order. Liao, Keen, and Powell (Ref. 23) found that a 0.75 mm diameter point gave a current ten times that of a needle point. They also found that a fiber phonograph needle that had been wetted to make it conducting gave ten times the current of the 0.75 mm diameter tip. A flat end on a needle instead of a point might have a strong field around the circumference of the tip, giving more current. Using a material like thoriated tungsten, which readily emits electrons might also increase the current. It is possible that irradiating the discharge region, either with ultraviolet light, or ionizing γ radiation from thorionite ore, as was used very early on in corona research (Ref. 24), might make a difference, but at an added level of complexity, making this an unattractive option. Thus there are additional approaches to pursue to increase the current and hence thrust. Pulsing the excitation voltage appeared to offer the best hope for improvement, but this was not clearly demonstrated, and in any case does not appear to offer the orders of magnitude improvement in thrust per unit power that is needed.

In addition to these problems, there are unaddressed questions about the practicality of a corona discharge thrust source, namely.

(1) Will the needle electrodes stay sharp enough for any reasonable time? It was shown above that the pins used already eroded in a fairly short time.

(2) Can a rugged device be made that is still very light weight? Despite using foam board for the rig that was used, the rig weighed 1,477 g. Moreover, even at this weight, the rig was not very sturdy. The rig weight does not include the weight of any power supplies or high voltage switches: the smallest power supply used, the ultravolt, itself weighed 1,250 g, and so almost doubled the combined weight. However this power supply is well regulated, and also shielded, which is an unnecessary weight addition. A simpler power supply could conceivably weigh much less. The power supply is actually a converter of low voltage DC power, at 24 V to high voltage. This would be ideal for converting the output of a photovoltaic power source.

(3) The effect of forward velocity on the thrust has not been studied at all. It is quite possible that this will reduce the thrust.

(4) Reduction of thrust at lower pressure, i.e., altitude, has been demonstrated by Blaze Laboratories (Ref. 7). This is a serious disadvantage with a system that is likely to be marginal in thrust at sea level.

Conclusions

Although the goal of reaching 20 N/kW was reached, it was only reached at low values of thrust. The goal for ϕ was not reached. Based on this, and the considerations listed above, the use of a corona discharge for propulsion does not currently seem very practical. However, there are still avenues to pursue, such as the questions of tip shape and material. More research is needed to establish whether pulsed discharges could be more effective in generating thrust, and to address the issues raised above. Other types of electric discharges, e.g., dielectric barrier discharges (Refs. 25 and 26), also generate an ionic wind, and should be considered for their propulsion potential.

References

1. Chattock, A.P., "On the Velocity and Mass of the Ions in the Electric Wind in Air," *The Philosophical Magazine*, Fifth Series, vol. 48, no. 294, pp. 401–421, (1899).
2. Stuetzer, O.M., "Ion Drag Pumps," *Journal of Applied Physics*," vol. 31, no. 1, pp. 136–146, (1960).
3. Christenson, E.A., and Moller, P.S., "Ion-Neutral Propulsion in Atmospheric Media," *AIAA Journal*, vol. 5, no. 10, pp. 1768–1773, (1967).
4. Helios web site: www.nasa.gov/centers/dryden/news/FactSheets/FS-068-DFRC.html
5. Sirak, M., "Lockheed Martin Wins Airship Competition," *Jane's Defense Weekly*, 6 October, 2003.
6. Lowe, J.D., "Large Crane Airships: Design and Dynamics," AIAA paper 87–2378, (1987).
7. Blaze Laboratory web site: www.blazelabs.com
8. Bortnikov, Yu. S., Nesterov, V.A., Rubashov, I.B., and Chaplii, V.I., "CORONA DISCHARGE IN AN AIR STREAM," *Soviet Physics-Technical Physics*, vol. 14, no. 11, pp. 1579–1582, (1970).
9. Cobine, J.D., "Gaseous Conductors," Dover Publications, Inc., New York, 1958.
10. Tyndall, A.M., and Grindley, G.C., "The Mobility of Ions in Air. Part I. Negative Ions in Moist Air," *Proceedings of the Royal Society (London)*, vol. 110, no. 754, pp. 341–358, (1926).
11. Sigmond, R.S., "Simple approximate treatment of unipolar space-charge-dominated coronas: The Warburg law and the saturation current," *Journal of Applied Physics*, vol. 53(2), February 1982, pp. 891–898.
12. Brown, T.T., "Electrokinetic Apparatus," *U.S. Patent* 3,187,206, June 1965.
13. Talley, R.L., "Twenty First Century Propulsion Concept," *U.S. Air Force Propulsion Directorate, Final Report* PL-TR-91-3009, May 1991.
14. Bahder, T.B., and Fazi, C., "Force on an Asymmetric Capacitor," *Army Research Laboratory Report* ARL–TRL–3005, March 2003.
15. Tajmar, M., "Bielefeld-Brown Effect: Misinterpretation of Corona Wind Phenomena," *AIAA Journal*, vol. 42, no. 2, pp. 315–318, February, 2004.
16. Naudin, J-P., web site: http://jnaudin.free.fr
17. Persson, K-B., "Brush Cathode Plasma—A Well-Behaved Plasma," *Journal of Applied Physics*, vol. 36, no. 10, pp. 3086–3094, October 1965.
18. Raiser, Yu. P., "Gas Discharge Physics," Springer-Verlag, New York, 1991.
19. Loeb, L.B., "Fundamental Processes of Electrical Discharge in Gases," John Wiley & Sons, New York, 1939.
20. http://www.ansoft.com/products/em/maxwell
21. de Seversky, A.N.P., "Ion Propelled Aircraft," *Popular Mechanics*, August 1964.
22. Riley, J.P., "Pulser/sustainer electric-discharge laser," *Journal of Applied Physics*, vol. 43, no. 8, pp. 3411–3416, August 1972.
23. Liao, T.W., Keen, W.A. Jr., and Powell, D.R., "Relationship Between Corona and Radio Influence on Transmission Lines, Laboratory Studies l—Point and Conductor Corona," *Trans. AIEE*, New York, paper 57–167, January 21–25, 1957.
24. Amin, M.R., "Fast Time Analysis of Intermittent Point-to-Plane Corona in Air, I. The Positive Point Burst Pulse Corona," *Journal of Applied Physics*, vol. 25, no. 2, pp. 210–216, February, 1954.
25. Moreau, E., "Airflow Control by Nonthermal Plasma Actuators," *J. Phys.D:Appl. Phys.* vol. 40, pp. 605–636, 2007.
26. Corke, T.C., Post, M.L., and Orlov, D.M., "SDBD Plasma Enhanced Aerodynamics: Concepts," Progress in Aerospace Sciences, vol. 43, pp. 193–217, 2007.

REPORT DOCUMENTATION PAGE			Form Approved OMB No. 0704-0188

1. REPORT DATE *(DD-MM-YYYY)*	2. REPORT TYPE	3. DATES COVERED *(From - To)*
01-12-2009	Technical Memorandum	

4. TITLE AND SUBTITLE
An Investigation of Ionic Wind Propulsion

5a. CONTRACT NUMBER

5b. GRANT NUMBER

5c. PROGRAM ELEMENT NUMBER

6. AUTHOR(S)
Wilson, Jack; Perkins, Hugh, D.; Thompson, William, K.

5d. PROJECT NUMBER

5e. TASK NUMBER

5f. WORK UNIT NUMBER
WBS 561581.02.08.03.13.05

7. PERFORMING ORGANIZATION NAME(S) AND ADDRESS(ES)
National Aeronautics and Space Administration
John H. Glenn Research Center at Lewis Field
Cleveland, Ohio 44135-3191

8. PERFORMING ORGANIZATION REPORT NUMBER
E-17084

9. SPONSORING/MONITORING AGENCY NAME(S) AND ADDRESS(ES)
National Aeronautics and Space Administration
Washington, DC 20546-0001

10. SPONSORING/MONITOR'S ACRONYM(S)
NASA

11. SPONSORING/MONITORING REPORT NUMBER
NASA/TM-2009-215822

12. DISTRIBUTION/AVAILABILITY STATEMENT
Unclassified-Unlimited
Subject Categories: 07 and 75
Available electronically at http://gltrs.grc.nasa.gov
This publication is available from the NASA Center for AeroSpace Information, 443-757-5802

13. SUPPLEMENTARY NOTES

14. ABSTRACT
A corona discharge device generates an ionic wind and thrust, when a high voltage corona discharge is struck between sharply pointed electrodes and larger radius ground electrodes. The objective of this study was to examine whether this thrust could be scaled to values of interest for aircraft propulsion. An initial experiment showed that the thrust observed did equal the thrust of the ionic wind. Different types of high voltage electrodes were tried, including wires, knife-edges, and arrays of pins. A pin array was found to be optimum. Parametric experiments, and theory, showed that the thrust per unit power could be raised from early values of 5 N/kW to values approaching 50 N/kW, but only by lowering the thrust produced, and raising the voltage applied. In addition to using DC voltage, pulsed excitation, with and without a DC bias, was examined. The results were inconclusive as to whether this was advantageous. It was concluded that the use of a corona discharge for aircraft propulsion did not seem very practical.

15. SUBJECT TERMS
Ion propulsion; Air breathing engines; Electric corona

16. SECURITY CLASSIFICATION OF:			17. LIMITATION OF ABSTRACT	18. NUMBER OF PAGES	19a. NAME OF RESPONSIBLE PERSON
a. REPORT	b. ABSTRACT	c. THIS PAGE			STI Help Desk (email:help@sti.nasa.gov)
U	U	U	UU	42	19b. TELEPHONE NUMBER *(include area code)* 443-757-5802